Πανεπιστήμιο Κρήτης
Σχολή Θετικών Επιστημών
Τμήμα Φυσικής

ΜΕΤΑΠΤΥΧΙΑΚΟ ΠΡΟΓΡΑΜΜΑ ΟΠΤΟΗΛΕΚΤΡΟΝΙΚΗΣ - ΜΙΚΡΟΗΛΕΚΤΡΟΝΙΚΗΣ

Μεταπτυχιακή Εργασία

ΚΑΤΑΣΚΕΥΗ ΤΡΙΣΔΙΑΣΤΑΤΩΝ ΜΙΚΡΟΔΟΜΩΝ ΒΙΟΛΟΓΙΚΩΝ ΜΟΡΙΩΝ

Δρακάκης Θεόδωρος

Επιβλέπων: Καθ. Κ. Φωτάκης
Υπεύθυνοι Εργασίας: Δρ.Μ.Φαρσάρη
Δρ. Γ. Φιλιππίδης

Ηράκλειο 2006

University of Crete
School of Sciences
Department of Physics

Postgraduate Course in Microelectronics and Optoelectronics

Master Thesis

FABRICATION OF 3D BIOMOLECULAR MICROSTRUCTURES

Theodore Drakakis

Supervisor: Prof. C. Fotakis
Advisors: Dr.M.Farsari
Dr. G.Filippidis

Ευχαριστίες

Η παρούσα εργασία είναι αποτέλεσμα συνεργασίας πολλών ανθρώπων τους οποίου θα ήθελα να ευχαριστήσω για την ευγενική προσφορά τους. Καταρχήν θα ήθελα να ευχαριστήσω τον κ. Κωνσταντίνο Φωτάκη πρόεδρο του Ι.Η.Δ.Λ. του Ι.Τ.Ε ,ο οποίος μου έδωσε την ευκαιρία να εργαστώ στα εργαστήρια λέιζερ κατά τη διάρκεια διεκπεραίωσης των πειραμάτων.

Στη συνέχεια θα ήθελα να ευχαριστήσω ιδαίτερα την κα. Μαρία Φαρσάρη και τον κο. Γιώργο Φιλιππίδη ερευνητές του Ι.Η.Λ.Δ για την πολύτιμη συνεργασία τους , γιατί υποστήριξαν υλικά και επιστημονικά την εργασία αυτή και τέλος γιατί μου έδωσαν την ευκαιρία να ασχοληθώ με μία νέα μέθοδο τον Πολυφωτονικό Πολυμερισμό για τον σχηματισμό μικροδομών. Τέλος, θα ήθελα να ευχαριστήσω τους κ.Παναγιώτη Τζανετάκη και κ. Σάββα Γεωργίου που δέχτηκαν μαζί με τον κ. Κωνσταντίνο Φωτάκη να συμμετέχουν στην τριμελή επιτροπή του μεταπτυχιακού μου διπλώματος.

Επίσης να ευχαριστήσω την κα. Ηλέκτρα Γκιζελή του τμήματος Βιολογίας του Πανεπιστημίου Κρήτης γιατί μου πρόσφερε την δυνατότητα να ασχοληθώ με τον τομέα των Ακουστικών Βιοαισθητήρων . Να ευχαριστήσω ακόμα τον Γιώργο Παππαδάκη και τον Μιχάλη Σαϊτάκη για την άμεση συνεργασία που είχαμε στο εργαστήριο των Βιοαισθητήρων, για την ενθαρρυντική τους στάση και την πραγματική πολύτιμη βοήθειά τους .

Ακόμα ,θα ήθελα να ευχαριστήσω τον κο Αποστόλη Εγγλέζη και την Αντωνία Μπονάρου για την ,επι καθημερινής βάσεως συντήρηση αλλά και την επίλυση προβλημάτων του λέιζερ .

Βέβαια ,πριν κλείσω το μέρος αυτό ,ευχαριστώ θερμά τους φίλους μου Αλέξανδρο και Βασίλη Σελίμη, Γιώργο Δημητρακάκη, Νίκο Ψυλλάκη ,Χρήστο Ζηδιανάκη ,Μανόλη Βαβαδάκη, Γιώργο Βασιλάκη ,Μανόλη Χαριτάκη ,Θανάση Λαμπράκη, Ντίνο Ξεζωνάκη, Μανόλη Πάτερο, Μανόλη Ανωγειανάκη και Νίκο Καμπιτάκη για την υπομονή τους όλα αυτά τα χρόνια, για την συμπαράστασή τους σε δύσκολες στιγμές που βίωσα και γιατί με τιμούν με την φιλία τους.

Τέλος το μεγαλύτερο ευχαριστώ νιώθω την ανάγκη να το πω στην οικογένειά μου ,που μπορεί να μη βοήθησαν στα πειράματα

αλλά με στήριξε και με στηρίζει με υπομονή και κατανόηση όλα αυτά τα χρόνια .

Στους γονείς μου

Abstract

We demonstrate a novel method for three-dimensional patterning of proteins and other biological molecules. The technique is based on multi-photon polymerization of photosensitive composites and biotin-avidin chemistry. This technique opens the way for the fabrication of structures with a wide range of biomaterials, as well as studying their dynamics within complex 3D structures.

For the fabrication of the 3D structures, multiphoton polymerisation is used. Multiphoton polymerization of photo-sensitive polymers is a very promising approach for the fabrication of complicated three-dimensional microstuctures. Compared with projection lithography (photo, x-ray and electron beam) and soft lithography technologies, multi-photon photopolymerization is unique in its 3D processing capability. When femtosecond laser pulses are tightly focused into the volume of a photosensitive resin, which is transparent in the infrared, the liquid is photopolymerized into solid state by absorbing more than one photons. This process is confined to a highly localized area at the focal point due to the nonlinear dependence of the polymerisation rate on the laser intensity. However to establish this technology as a micro –processing tool , a lot of work on optics , materials and electronic controlling has been done to reduce the writing laser power ,and improve the fabrication accuracy and efficiency.

Biotin is subsequently attached to the 3D structures via UV-activated cross-linking. The integrity of the photolytically immobilized biotin is confirmed by detecting the binding of fluorescently labeled avidin via fluorescence.

For monitoring the loading of photobiotin to the photopolymer and for quantification of the measurements , an acoustic sensor technique is used. This system, known as the Love wave device, incorporates a shear horizontal-surface acoustic wave (SH-SAW) overlaid by a thin polymer layer. The polymer layer acts as a waveguide through surface-energy confinement and enhances the sensitivity of mass deposition. Mass adsorbed to the

polymer surface changes the phase of the waves during the adsorption process.

Finally the SAW technique has used to examine the attachment of biotinylated anti-human IgG antibody. A permanent phase change has again been measured, indicating the functional operation of the photobiotin-avidin complex.

Table of Contents

Chapter 1 Introduction

The analysis of biological samples with biosensors has been the focus of much analytical research in recent years. Micro-patterned surfaces have become increasingly important to biosensor systems, with patterned arrays of antibodies, DNA, enzymes and supported lipid membranes proposed to monitor the functions of biomolecules and cells *in situ* [1]. The construction of arrays of micrometer dimension allows the measurement of many different biological analytes using samples of very small volume. Furthermore, such structures enable the investigation of the dynamics of biomaterials in scales typical of the confined cytoplasm and nucleus [2].

A number of different approaches have been examined for fabricating patterned biological polymer surfaces [3], photoactivation of light sensitive molecules being one of them [4]. The use of photoactive biotin derivatives is an attractive technique, as it not only offers the exploitation of a strong non-covalent biological interaction between biotin and the glycoprotein avidin, but also it allows binding of biotinylated ligands, enabling the fabrication of multi-functional assemblies of molecules upon the sample surface [5].

Almost in all cases, biomolecule patterning has been two-dimensional (2D). Three-dimensional (3D) patterning on the basis of DNA complex structures has been demonstrated [6], but requires extensive biochemical facilities that are not available except to specialized labs. We demonstrate a method of 3D biotin-avidin patterning which enables the construction of arbitrary two and three dimensional shapes, not restricted to array-based shapes. By going from 2D to 3D one can increase greatly the active surface area and thus the sensitivity of the system without sacrifices to the size. The method allows not only prototyping but direct device construction.

For the fabrication of the 3D nanostructures, we use the biocomaptible organic-inorganic hybrid ORMOCER, which is characterized by high transparency in the visible and near infrared ranges above 400 nm [7] and therefore allows three-photon

polymerization using a 1.028 μm laser. The construction of 3D structures has been carried out using non-linear optical stereolithography, a technique that allows the fabrication of three-dimensional structures with sub-micron resolution [8].

Biotin is subsequently attached to the 3D structures via UV-activated cross-linking. Biotin is subsequently attached to the 3D structures via UV-activated cross-linking. The integrity of the photolytically immobilized biotin is confirmed by detecting the binding of fluorescently labeled avidin via fluorescence. The 3D structures fluoresce very strongly when excited with green light and this fluorescence originates solely from the 3D component, and not from the glass substrate. Since ORMOCER and photobiotin do not fluoresce in the green, fluorescence can be safely ascribed to the streptavidin.For the samples which are not pre-treated with photobiotin and only treated with avidin there was no fluorescence. Therefore, the incorporation of avidin is due to the biotin bound to the structure. Similarly, no fluorescence is detected if in the procedure biotin instead of photobiotin is employed. This result demonstrates that the biotin and avidin are not simply incorporated within a porous structure; instead, chemical bonding is clearly involved. Upon UV irradiation, photobiotin is known to generate a reactive biotin [9]. It is likely that this intermediate reacts with dangling Si-O bonds at the surface of the polymerized structure.

For monitoring the loading of biotin to ORMOCER, an acoustic sensor technique has been used based on a waveguide geometry. This system, known as the Love wave device, incorporates a shear horizontal-surface acoustic wave (SH-SAW) device overlaid by a thin polymer layer; the latter acts as a waveguide through surface-energy confinement and enhancement of sensitivity to mass deposition. [10]. For biosensing experiments, mass adsorbed to the polymer surface can be monitored in real time by following the phase change of the wave during the adsorption process.

The manuscript is divided in two main parts. In the chapters of the first part the basic theory is presented, while in the chapters of the second part the results of the experimental work and the future plans are presented. The first part contains three chapters.

In Chapter 2 we begin with a brief introduction to multi-photon absorption and photopolymerization.
In Chapter 3 we carry on with the presentation of the theory of Acoustic Biosensors. Basic magnitudes, like piezoelectricity and Love waves propagation are introduced. We briefly discuss the temperature, pressure and flow rate effects on the control of the sensor environment.
In Chapter 4 we present extensively the basic characteristics of the materials that we used during the experiments. First, ORMOCER is examined for its mechanical and optical properties and for its three photon polymerization. Second, an acrylate-based photo-polymer sensitized with Eosin Y dye is examined for its two photon polymerization. Third, the system of photobiotin-avidin is presented. Finally, protein IgG is examined in detail.
The second part of this thesis contains three chapters.
In Chapter 5 the developed experimental facility for two and three photon polymerization is analyzed. The laser system, the optical components including the mechanical scanning system, as well as the piezoelectric stage are described in full detail. Finally we demonstrate the tracing of biomolecules interaction using a Fluorescence Microscopy.
In Chapter 6 we mention the tracing of biomolecules interaction using an acoustic technique. The results of the experiments with ORMOCER, polystyrene and IgG are presented .
Finally, in Chapter 7, conclusions and plans for future work are discussed.

Chapter 2 Multi-Photon Absorption and Polymerization

Introduction

Femtosecond laser interaction with matter differs essentially from those with longer pulses or CW lasers in its significant nonlinearity, ultrafast characteristics and the possibility of highly localization of reaction volume. The multi-photon photopolymerization technology is expected to play a similar role to that played by lithography for planar semiconductor device processing, but for micro-nanofabrication of 3D polymer-based optoelectronic devices as well for microelectromechanical systems.

The emergence of a new technology in 1997, two-photon photopolymerization(2PP) [11], has brought the light curable resin into the realm of nanofabrication. As indicated by the name, the resins are polymerized not by absorbing one UV photon, but by simultaneously absorbing two photons at longer wavelength, usually in the red-infrared (IR) spectral region. The two-photon process [12–13] has at least two advantages compared to single-photon absorption used in conventional rapid prototyping. First, common polymers have negligible linear absorption in the rednear- infrared (NIR) region, so the laser penetrates deeply into materials and directly induces polymerization from inside without contaminating outside of the focal volume. Secondly, the quadratic dependence of polymerization rate on the light intensity enables 3D spatial resolution, and the accuracy is better than that achieved in single photon process.

In addition three photon photopolymerization(3PP) is initiated through the non linear process of three-photon absorption of a photoinitiator , and induces several chemical reactions between starter molecules and monomers in a transparent resin . 3PP is a process which allows the fabrication of components of very high resolution . 3PP was experimentally reported for the first time in 2005 by M.Farsari,G.Filippidis and C.Fotakis for fabrication microstructures with high resolution .

A Two Photon Photopolymerization and Applications

2.1 Two Photon Photopolymerization

Two-photon photopolymerization was experimentally reported for the first time in 1965 by Pao and Rentzepis [14] as the first example of multiphoton excitation-induced photochemical reactions. They focused 694-nm laser from a pulsed Ruby laser into a sample of styrene that was cooled to 77 K. After developing in methanol, solid precipitate was extracted and confirmed to be polystyrene through IR absorption. In the particular experiment, no photosensitizer was used and the author tried to increase the two photon absorbance by using monomers with added functional groups, such as para-isopropylstyrene and chlorine-substituted derivatives of styrene. As a result, much enhanced two-photon polymerization was observed.

Two-photon photopolymerization has unique merits:

– First of all, it has intrinsic ability to produce 3D structures. In addition, the long wavelength chosen for TPA has less absorption and less scattering, which gives rise to the deep penetration of light; use of ultrashort pulses can start intense nonlinear processes at relatively low average power, without
thermally damaging the samples.

– The two-photon photopolymerization system doesn't need vacuum condition for operation. The system is easy to operate and maintain.

No mask, mold, or stamp is needed for fabrication. It directly converts computer- designed patterns into matter structure. The rapid turnaround time for fabrication allows one to quickly iterate and modify design.

2.2 Material Processing with Femtosecond Lasers

2.2.1 Interaction of an organic medium with light

The interaction of an organic medium with light can be regarded within the framework of a dielectric subjected to an electric filed . In the dipole approximation ,the induced dipole momentum in a molecule due to the applied filed is given by

$$\mu_{ind} = -er \qquad 1$$

where e is the electronic charge and r is the filed induced displacement .The bulk polarization resulting from this induced dipole moment is given by

$$P_{ind} = -Ner \qquad 2$$

where N is the electron density in the medium .In these cases (where the field strength is low),to a good a approximation ,the induced polarization P_{ind} in a medium ,due to the applied electric field E is linear in E and can be written as

$$P_{ind} = X^{(1)}E \qquad 3$$

where $X^{(1)}$ is a susceptibility and is a second rank tensor and has 9 components because it relates all the components of the polarization vector with all components of the electric field vector .The optical response of a medium at an optical frequency ω is represented equivalently by the complex refractive index n_c given by

$$n_c^2(\omega) = 1 + 4\pi\omega X^{(1)} \qquad 4$$

The complex refractive index can be written as the sum of the real and imaginary part as

$$n_c = n + ik \qquad 5$$

where n the real part which corresponds to the dispersion of refractive index ,while k the imaginary part which corresponds to an electronic absorption.

This can be understood by considering the medium to be an assembly of forced harmonic oscillators which are driven by sinusoidal optical field .The oscillators also experience a damping force which can be interpreted as an exchange of energy between the optical field and the medium .Using the harmonic oscillator model,we get an equation of motion .

$$\frac{d^2x}{dt^2} + 2\Gamma\frac{dx}{dt} + \omega_0^2 x = -\frac{e}{m}E \qquad 6$$

where Γ is the damping constant .Considering a sinusoidal electric field

$$E(t) = \frac{1}{2} E_0 \left[e^{i\omega t} + e^{-i\omega t} \right] \qquad 7$$

The solution to this differential equation are

$$n = \mathrm{Re}\, n_c = 1 - \frac{Ne^2}{m} \frac{2\pi\left(\omega^2 - {\omega_0}^2\right)}{(\omega^2 - {\omega_0}^2)^2 + (2\Gamma\omega)^2} \qquad 8$$

$$k = \mathrm{Im}\, n_c = \frac{Ne^2}{m} \frac{4\pi\Gamma\omega}{(\omega^2 - {\omega_0}^2)^2 + (2\Gamma\omega)^2} \qquad 9$$

The real part of the refractive index corresponds to dispersion while the imaginary part corresponds to absorption .

2.2.2 Non linear Optical Effects

The treatment of the previous section assumed the medium to be a collection of harmonic oscillators .This assumption is valid only for small displacement from the equilibrium position .If the field is strong enough as in our case ,the equation of motion will contain non harmonic terms . Equation 6 must be modified to

$$\frac{d^2x}{dt^2} + 2\Gamma\frac{dx}{dt} + \omega_0^2 x + ax^2 + bx^3 + \ldots\ldots\ldots = -\frac{e}{m}E \qquad 11$$

If the diversion in harmony is small compared to the linear term, the solution can be approximated as a power series in E .
The value of material polarization P is:

$$P = \chi^{(1)}E + \chi^{(2)}E^2 + \chi^{(3)}E^3 + \ldots\ldots\ldots \qquad (12)$$

where the quantities of $x^{(1)}$, $x^{(2)}$, $x^{(3)}$ are first ,second-and third- -rank tensors, representing linear, second-order and third-order optical susceptibilities. $X^{(2)}$ gives rise to second order nonlinear effects such as optical rectification ,second harmonic generation ,and linear electro-optic effect . $X^{(3)}$ is responsible for third-order

effects such as optical Kerr effect,electric field induced second harmonic generation, four wave mixing, third harmonic generation and two photon absorption. In resonant processes, there is no contribution from the even-order susceptibilities like $\chi^{(2)}$ and $\chi^{(4)}$. Therefore, the nonlinear absorption is described by the imaginary parts of $\chi^{(3)}$, $\chi^{(5)}$ of which typical effects are two-photon and three-photon absorptions, respectively.

Nonlinear processes [15,16], for example, multiphoton absorption including two-photon absorption (TPA) [16,17], have come to play a dominant role in nanofabrication. In order to produce a lasting effect on a material, photons must first be absorbed. The energy and momentum are exchanged between the optical fields and molecules through absorption and emission. In such a process, the imaginary part of nonlinear susceptibility represents the energy transfer from the light field to a medium. The energy exchanged between the light beam and the medium per unit time and unit volume is:

$$\frac{dW}{dt} = \left\langle \vec{E} \cdot \dot{\vec{P}} \right\rangle \qquad (13)$$

where E is the electric field vector and the brackets denote time average over several cycles of the field .

Particularly, for degenerate TPA, that is, the process of photons of identical energy are simultaneously absorbed, the energy absorption rate is:

$$\frac{dW}{dt} = \frac{8\pi^2\omega}{c^2 n^2} I^2 \,\mathrm{Im}[\chi^{(3)}] \qquad (14)$$

It is seen that the TPA rate quadratically depends on the light intensity, which is an important mechanism to improve the spatial resolution in two-photon fabrication. Typical values of intensity are 10^{20}photons/cm^{2}sec . Something proportional matters in chemical reactions like 2A+B->C where the rate of this reaction depends quadratically on the concentration of A .

2.2.3 Cross section of 2PA

Two photon absorption is often described in terms of a cross section σ_2 .A high capability of materials to absorb photons via TPA is desired, which is described by TPA cross-section, σ_2, defined by

$$\frac{dn_p}{dt} = \sigma_2 N F^2 \qquad (15)$$

where N and dn_p/dt are the number of absorbing molecules per unit volume and number of absorbed photons per unit time respectively. F=I/hn denotes photon flux. According to Eq 15, the TPA cross-section is:

$$\sigma_2 = \frac{8\pi^2 h\nu^2}{c^2 n^2 N} I^2 \,\mathrm{Im}[\chi^{(3)}] \qquad (16)$$

Two Photon cross-section can also be expressed in terms of the change in intensity of an incident laser beam .

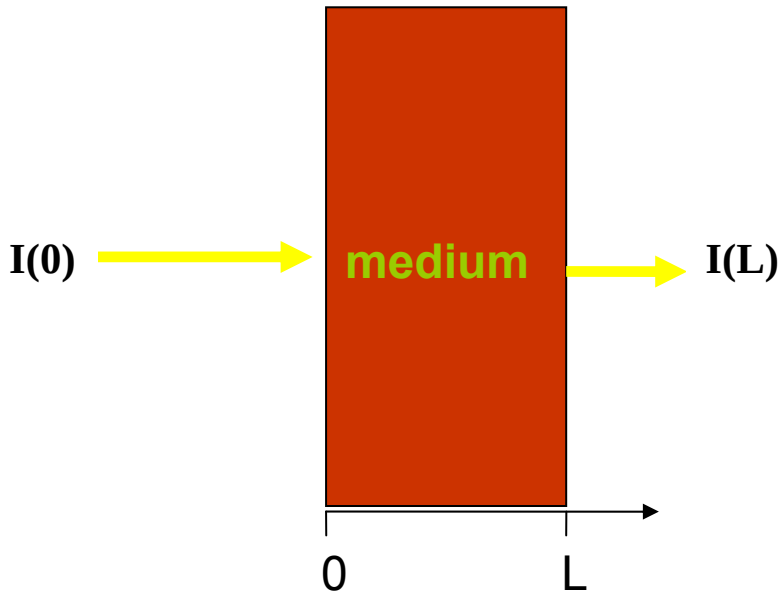

Fig 1 Change in intensity of a beam as it propagates through a medium

The change in intensity I of a beam as it propagates through a medium with linear and two photon absorption is given by

$$\frac{dI}{dz} = -(a_1 I + a_2 I^2) \qquad 17$$

where a_1 is the linear absorption coefficient and a_2 is the two photon absorption coefficient related to the imaginary part of the third order susceptibility $x^{(3)}$.
For a beam with a rectangular temporal profile and a Gaussian spatial profile and for a medium with no linear attenuation (a_1=0), the transmitted intensity I(L) can be shown to be

$$I(L) = \frac{1}{La_2}[\ln(1 + I_0 La_2] \qquad 18$$

where I_0 is the incident intensity and L is the thickness of the sample. The molecular two photon absorption cross section σ_2 is related to a_2 by

$$hva_2 = \sigma_2 N_0 = \sigma_2 N_A d_0 \times 10^{-3} \qquad 19$$

where hv is the incident photon energy N_0 is the molecular density (cm^{-3}) , N_A is the Avogadro number and d_0 the concentration,(mol l^{-1}).

2.2.4 Computation of multophoton absorption coefficients at the molecular level

For the calculation of nonlinear coefficients we use the sum over states method which is based on a pertubative expansion of the stark energy .The optical nonlinearities are introduced as a result of Stark mixing with various excited states .

For one photon transitions the most important quantity for one photon transitions is the transition moment $M_{0f} = \langle 0|r|f\rangle$,where $|0\rangle$ and $|f\rangle$ are the wave functions of the initial and final states involved in the transition ,respectively .For a two photon absorption transition ,the expression for the cross section contains terms of the type $M_{0i}M_{if}$

where i stands for the intermediate time-dependent state involved in the transition . Then the quantity that is important for two photon transitions is the transition tensor S_{0f} given

$$\left|S_{f0}(\lambda,\mu)\right|^2 = \left|\sum_i^N \left[\frac{(\lambda\langle i|r|0\rangle)(\langle f|r|i\rangle\mu)}{E_i - E_\lambda + i\Gamma} + \frac{(\mu\langle i|r|0\rangle(\langle f|r|i\rangle\lambda)}{E_i - E_\mu + i\Gamma}\right]\right|^2 \qquad 20$$

where λ and μ are the unit vectors defining the polarizations of the two photons in the laboratory coordinates ,0 and f are the ground electronic state and the final excited state ,and i is one of the N intermediates states .The terms $\langle i|r|0\rangle$ and $\langle f|r|i\rangle$ are the transitions moments for the 0->i and i->f transitions. E_λ and E_μ are the energies of the two photons respectively and E_i and Γ_i are the energy and linewidth corresponding to the ith intermediate state respectively . In terms of the transition tensor , the basic cross section for TPA is given by the expression .

$$\sigma_2 = \frac{(2\pi e)^4}{(ch)^2}\left[E_\lambda E_\mu g\left(E_\lambda + E_\mu\right)\right]\left|S_{f0}(\lambda,\mu)\right|^2 \qquad 21$$

where g is the line shape function and is Gaussian

The design of molecules that have a large TPA cross-section is an important task of stereolithography using two-photon photopolymerization. First, a femtosecond laser carries much greater peak power. With conventional light sources the strength of the light field is in the range of 1 V/cm and the resulting elongation of dipole is smaller than 10^{-16} m, much smaller than atomic or molecular diameters (10^{-10}~10^{-7} m). With femtosecond laser irradiation, the field strength is 10^8 V/cm, which corresponds to an incident light intensity of 100GW/cm^2 and is sufficient to induce direct bond breaking

.Two photon absorption has an extremely small cross-section, it is confined to occur only in a small 3D volume around the close vicinity of the laser focus, less than the cubic wavelength (λ^3). Typical values for TPA cross section are 10^{-48} -10^{-50} cm^4 sec/photons. Hence, a quite high 3D spatial resolution can be achieved in the pinpoint exposure. Secondly, when materials are irradiated with femtosecond laser pulses, the photon energy is deposited much faster than electrons could transfer it to the lattice,

or molecule/ atom oscillations through phonon emission, meaning that the excitation is a heat insulation process [17,18,19].

2.3 Fundamentals of Stereolithography using Two-Photon Photopolymerization

Photopolymerization is one of the most important types of photochemical reactions that have been used for laser fabrication [21]. This is because the material resins undergo a significant phase transition after laser irradiation, from liquid to solid, and non-polymerized liquid is easily removed by a developing process so that solidified 3D structures stand out [20].The basic components of the starting liquid material are monomers and oligomers (or prepolymer). Upon light excitation, the monomers or oligomers may be solidified by two means: polymerization and crosslinking [21].

2.3.1 Descriptions of polymerization based on radical initiators.

An important feature of polymerization is the chain reaction by which macromolecules are created, while cross-linking is concerned more with the formation of crosslinks with chemical bonds . An important difference of these two kinds of reaction lies in their quantum yield, which is defined as the ratio of number of polymerized monomer units to the number of photons that are needed to cause this polymerization.

In the case of photocrosslinking, addition of each monomer unit requires absorption of a photon, leading to a quantum yield less than 1.

In contrast, photopolymerization is realized via chain reactions as shown in the following equation (Eq. 1), so the quantum yield can reach several thousands .

$$M \xrightarrow{M} M_2 \xrightarrow{M} M_3 \ldots\ldots M_{n-1} \xrightarrow{M} M_n \qquad 1$$

Here M is the monomer or oligomer unit, and M_n, the macromolecule containing n monomer units. The quantum yield of general monomers and oligomers is low. In order to increase the

initiating efficiency, one or several low-weight molecules that are more sensitive to light irradiation are added. They form initiating species of radicals or cautions by absorbing photons. Such small molecules are called photoinitiators.

$$I \xrightarrow{2h\nu} I^{*} \longrightarrow R\bullet \qquad 2$$

where symbols denote photoinitiator (I), radical (R·) and I*, an intermediate state of the photoinitiator after absorbing a photon.

$$R\bullet + M \rightarrow RM\bullet \xrightarrow{M} RMM\bullet\bullet \rightarrow RM_n\bullet \qquad 3$$

The photoproduced radicals react with monomers or oligomers, producing monomer radicals, which combine with new monomers, and so on, so the monomer radicals expand in a chain reaction, until two radicals meet with each other. This chain propagation stops in either of the following channels:

$$RM_n\bullet + RM_m\bullet \rightarrow RM_{m+n}R \qquad 4$$

$$RM_n\bullet + RM_m\bullet \rightarrow RM_n + RM_m$$

Therefore the polymerization process consists of several steps: (i) photoinitiation, (ii) chain propagation and (iii) termination.

A good photoinitiator should be (i) easily reduced to an initiating species upon light irradiation, and (ii) provide photoproduced radicals or cautions active enough to react with monomers or oligomers.

The nonlinear response of photopolymerization is caused by highly reactive oxygen molecules absorbed by resin. Oxygen molecules inhibit polymerization reaction at the beginning of polymerization, because oxygen molecules scavenge the radicals that generate the polymerization reaction. Accordingly, when the intensity of light is adequately low, polymerization reaction does not propagate, because almost all the photons are consumed by the oxygen molecules.

A photosensitizer is a molecule that absorbs light and then transfers the energy to a photoinitiator. With such a scheme, the photoinitiation process is expressed as:

$$S \xrightarrow{hv} S^* \ldots \xrightarrow{I} I^* \rightarrow R^{\bullet} \quad 5$$

where S is the photosensitizer. A co-initiator itself doesn't absorb light, but it is involved in the production of radical species. Reactions that are typically used for laser fabrication are : double-bond addition of acrylates (radical-type)

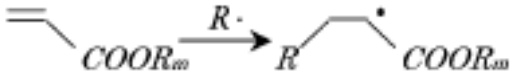

6

For a radical type initiator, benzoyl is the most widely used chromophore, which must have the initiator ,since it exhibits good absorption in the UV region.

After polymerization, the oligomer constitutes the backbone of the polymer network. The physical, chemical and mechanical properties of the solidified resin strictly depend on the nature and structure of the oligomer. Oligomers generally contain at least two reactive groups, from which both cross-linking and polymerization could occur.

Monomers have a much smaller molecular weight and consist of one or several reactive groups . They polymerize similarly to oligomers and are an important factor in determining the efficiency of polymerization. In addition, monomers are also useful for diluting resins so that the polymer is easier to handle for a particular use. For 3D micro-nanolithography, a suitable viscosity is of particular importance due to the opposite requirements in different steps of processing: a high viscosity is needed for keeping early produced volumes where they are created, while a low viscosity facilitates removal of unsolidified resin from intervals. For a successful fabrication the following behaviours are preferred: (i) high polymerization efficiency upon light irradiation, (ii) lower shrinkage after polymerization, (iii) fast reaction time and low dark polymerization.

2.3.2 Stepwise 2PA –Simultaneous 2PA

Selection rules for single-photon and two-photon excitation (2PE) are different, even parity transitions for 2PA and odd parity

transitions for one photon absorption. Electron excitations can occur stepwise or simultaneously as shown in Fig. 2a,b.

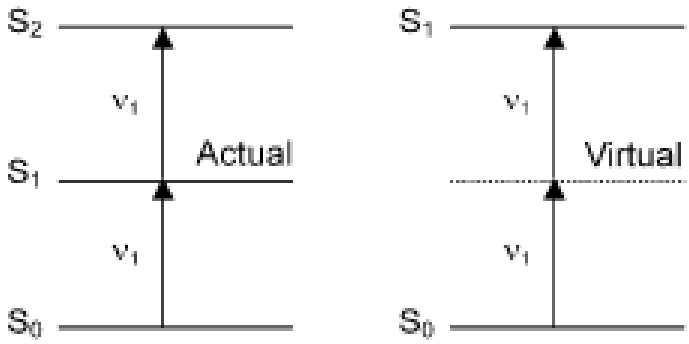

Fig. 2a,b Illustration of two-photon absorption schemes. a) stepwise 2PA with an actual intermediate energy level, and b) simultaneous 2PA with a virtual energy level.

The former could be treated as two sequential single-photon absorption processes and relies on the existence of a real intermediate state, from which an excited population is further pumped to a higher energy level by absorbing photons of the same energy as the ground state (excited state absorption). Such a process, although on some occasions also called 2PA or stepwise 2PA .

Simultaneous 2PA is a quantum mechanical three-body process, where an electron absorbs two photons simultaneously to transcend the energy gap in one excitation event [15]. As light passes through a molecule, a virtual state is formed when the first photon is absorbed. It persists for a very short duration (of the order of several femtoseconds as prescribed by Heisenberg_s Uncertainty Principle), which contrasts with the long lifetime of the actual intermediate energy level in stepwise absorption. 2PA can result if the second photon arrives before the decay of this virtual state. If the energy of the two photons are identical, the process is referred as degenerate 2PA, otherwise, the process is a non-degenerate one. For femtosecond laser micro-nanofabrication, simultaneous 2PA is more relevant.

However, since the transition probability of two-photon absorption tends to be extremely small, these processes generally require an expensive short-pulsed laser such as a Ti: Sapphire type.

2PA can be utilized for inducing photopolymerization. The difference between one-photon and two-photon induced photopolymerization lies in how the energy for activating initiators is provided.

2.3.3.High Efficiency Two-Photon Materials

Molecules of large TPA cross-section [22] are very important for the broad application of two-photon photopolymerization technology. Polar molecules were found to have a large change of dipole moment ($\Delta\mu$>10D) upon excitation from ground state to excited state [23]. Since both the ground and excited state can participate in the formation of the virtual energy level, the transition probability is proportional to $(\Delta\mu)^4$. For example TPA cross-section can be larger than $\sigma_2 \sim 10^{-50}$cm ^{4}s photon^{-1}.

One important effort in the molecular design of large σ_2 is searching for a molecular structure that potentially has larger $\Delta\mu$. It was found that π-conjugated systems such as those with phenylethenyl , fluorenyl [23], or polyenyl constructs were good candidates. In these molecules, electron- donating (D) and/or electron-withdrawing (A) moieties were separated by a conjugated π-electron system (A-π-A, D-π-D, D-π-A-π-D and A-π-D-π-A).

It is theoretically predicted and experimentally found [14] that σ_2 can be enhanced by increasing the conjugation length and the donor and acceptor strengths.

Another concern in two-photon molecule design is wavelength sensitivity [23]. This arises from the fact that the most suitable femtosecond laser is solid wavelength-tunable Ti:Sapphire laser, of which the wavelength ranges from 680 ~ 840 nm.

In addition for increasing TPA cross-section of chromophores, there is another route to enhance TPA by increasing the chromophore number density without causing aggregation.

2.3.4Dynamic Power Range

The polymerized voxel size increases with the increase of the irradiation duration (Δt) and the square of light intensity, SLI, (I^2). The dynamic power range is defined by the window between the

two photon polymerization threshold and the laser-induced breakdown threshold [14].

The photopolymerization threshold is determined by the production efficiency of initiating species from excited triplet states, which is characterized by the quantum yield of polymerization. The reactions that produce radicals should compete with monomer quenching, oxygen quenching and other pathways of deactivation of the excited states like phosphorescence emission. The threshold is also determined by the reactivity of radicals and monomers.

When laser irradiation is greater than a particular value, intense damage is induced in materials. This phenomenon is called laser-induced breakdown. The breakdown is dominated by a thermal process when pulse width is long (e.g. >10 ps for most transparent materials [14,15]

This was evidenced by observations that the breakdown threshold scales approximately with pulse width by $\tau^{1/2}$ for t >10 ps [15]. For shorter pulse widths(<1 ps), it is believed that the breakdown occurs in various materials via plasma generation [24]. Plasma can be produced via an avalanche process whereby free electrons are accelerated by the incident light field, causing an explosive cascade growth in electron density. The generated plasma can absorb and defocus the remaining incident light field. The breakdown causes the ablation process at sample surface and micro-explosion inside bulk, both accompanied by vaporization and atomization of the sample constituents.

Therefore, measures could be taken to increase the quantum yield of polymerization, and therefore the dynamic power range.
A simple and effective method is choosing laser wavelength so that radicals are produced more efficiently. It was experimentally observed [25] that the two-photon exposure threshold at 660 nm is roughly half of that at 700 nm, and approximately five times lower than that at 800 nm, while the breakdown threshold didn't vary significantly. The most efficient method is use of high TPA cross-section initiators.

2.4Advanced Techniques in Two-Photon Micro-Microfabrication

The progress of femtosecond laser technology and exploration of high efficiency photoinitiators and photosensitizers have fuelled the progress of two photon polymerization lithography. Its basic principle and potential applications have been demonstrated. However, to establish this technology as a micro-processing tool, a lot of work on optics, materials and electronic controlling has been done to reduce the writing laser power, evaluate and improve the fabrication accuracy and efficiency, and launch new applications.

2.4.1 Laser Diffraction Limit

Compared with projection lithography (photo, x-ray and electron beam) and soft lithography technologies, two-photon photopolymerization is unique in its 3D processing capability. However, the use of relatively long wavelength worsens the spatial resolution, for which the bottleneck is set by the optical diffraction limit . This is a limiting factor for the wide application of this technology. In this section, we will introduce how to avoid this problem and achieve SDL accuracy in 3D fabrication.

In two-photon 3D lithography, the Gaussian output of the laser undergo beam expansion and focusing, and is spatially filtered, producing a relatively flat wave front. Light distribution at the focal plane arises essentially from Fraunhoffer diffraction on the aperture of an objective lens , of which the diffraction pattern is shown by the (Fig. 3). The light intensity due to the constructive and destructive interference in the focal plane was assumed to follow a formula due to Airy :

$$I(x) = \left(2J_1(x)/x\right)^2 I_0 \qquad 1$$

where $x=2\pi aw/\lambda$, w is the coordinate in the diffraction pattern, and $I_o=ED/\lambda^2R^2$ is the intensity at the centre of the pattern, E is the total energy incident upon the aperture and $D=\pi\alpha^2$ is area of the aperture with an effective radius a.

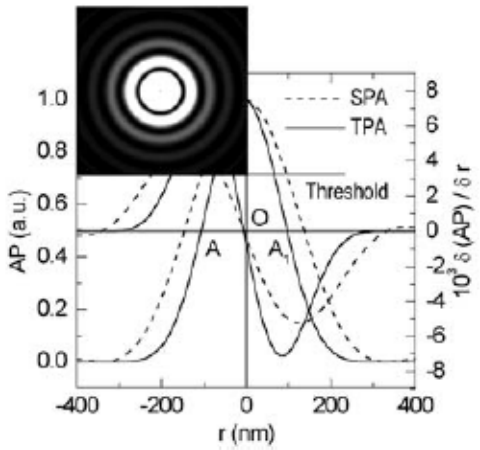

fig 3 Light intensity analysis for understanding the achievement of sub-diffraction-limit spatial resolution. Focal plane light intensity (dashed line) and the square of light intensity (solid line) distribution are associated with single-photon and two-photon excitation, respectively. Their derivative distribution is also shown. The inset is the diffraction pattern at the focal plane

For imaging, the resolving power was limited by Rayleigh's criterion, $r=k_1\lambda/NA$, due to the signal overlapping from neighbouring object points, where $k_1=0.4\sim0.6$ is a constant depending on the laser line width and projection geometry. The spatial resolution could be improved by utilizing either shorter wavelengths or larger NA focusing, but the diffraction limit cannot be circumvented.

For direct laser writing, a single focused beam is employed, producing an Airy pattern. The issue of light intensity overlapping is eliminated and the light intensity at the focal point was continuously adjustable. Therefore, even if the focal spot size is fixed for a given optical system (wavelength and objective lens), the diffraction limit can be circumvented, provided that the photochemical processes responsible for the formation of voxels have a threshold response to light excitation. Here the threshold was a level of light intensity (Fig. 3), above which the photochemical reactions become irreversible (for example, photopolymerized). In this case, the diffraction limit becomes just a measure of the focal spot size; it does not put any actual restraint on voxel sizes.

2.4.2 Thresholding Mechanism: Radical Quenching Effects

Thresholding performance depends on the individual mechanism of photochemical reactions. In radical type photopolymerization, oxygen molecules play an important role in the reaction process [33] Fig. 4. Oxygen quenches polymerization via two possible routes.

1)The first is triplet state quenching (T-quenching), where the triplet state of the initiator molecules can be directly consumed by reacting with oxygen molecules without generating any radicals.

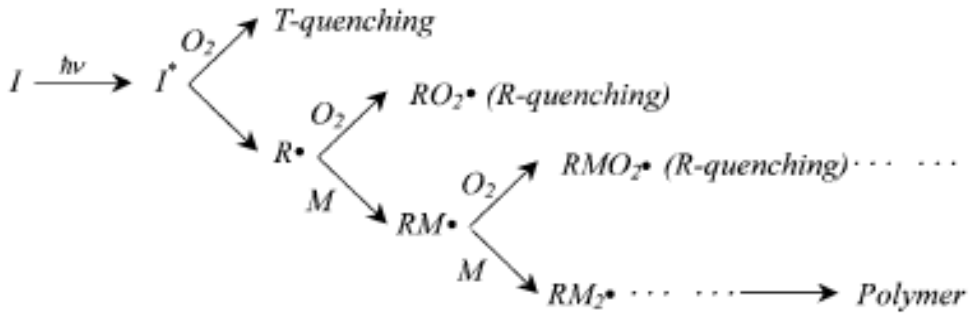

fig 4 Photopolymerization quenching by oxygen molecules under two mechanisms: triplet state quenching (T-quenching) and radical quenching (R-quenching). The latter is the major factor that works in the sub-diffraction-limit fabrication.

2)The second effect is radical quenching (R-quenching), where radicals combine with oxygen molecules, producing much less active peroxial radicals. This phenomenon, common in radical type polymerization, is the origin of the reaction induction period and it reduces polymerization efficiency .The two-photon photopolymerization threshold is closely related to the radical quenching effect. Due to the quenching effect, the existence of oxygen is generally considered as detrimental factor in polymerization.

By tailoring the light intensity at the focal volume, it is possible to reach a state where TPA-induced radicals survive and initiate polymerization only at the region where exposure energy is larger than the threshold. The intensity of high-order diffraction features (see the subsidiary maxima in the inset of Fig. 3) was low, and therefore easily controlled under the TPA threshold . Any chemical species that tends to prohibit photopolymerization

reactions, even in small concentrations, is called quencher. Oxygen is just one of many choices of quencher [26-28]

2.4.3 Two-Photon Excitation Related Focal Spots

When IR ultra-short laser pulses are tightly focused in a resin, initiators are decomposed into radicals by simultaneously absorbing two photons. The number of photons absorbed per molecule per unit time by means of TPA is proportional to the TPA cross-section,σ_2 and to SLI. The total number of photons absorbed per unit time is also a function of initiator concentration, C, and the volume V. In the absence of saturation and photobleaching, the number of radicals generated per unit time, N, is given by:

$$N = C\sigma_2\phi I_0^2 \int_V S^2(r,\vartheta,z)dV \qquad 2$$

where I_0 is the light intensity at the geometrical focal point, S(r,θ,z) is a unitless function used to describe the spatial distribution of the incident light, and φ is the quantum efficiency of radical yield.The shape of the TPE focal spot is determined by $S^2(r,\theta,z)$.

2.5 Applications of 2PP

Two-photon photopolymerization, a micro-nanotechnology still in its infancy and a subject of active research, has potential use in fields such as photonics, optoelectronics, biology, micro-machines and MEMS, and so forth. Among many, here we introduce applications that already have proof of concept.

1.Fabrication of PhCs

One of the most important applications of 2PP is the fabrication of PhCs. Photonic crystals (PhCs) [29,30] are microstructures with a periodical distribution of refractive indexes. They are the optical analogue of semiconductors, where a band gap is open due to the electron wave modulation by periodic

Coulombic potential. In a PhC, the multiple interference among waves scattered from each primitive unit may lead to a frequency region, called a photonic band gap (PBG), where light propagation in all directions is forbidden.

There are at least two advantages to fabricating PhCs using 2PP technology. First of all is the potential to produce PhCs of arbitrarily designed lattices. PhCs of varied lattice types, lattice constant, and filling factors are realizable just by scanning different CAD patterns. This simplicity in fabrication permits a systematic study of PhC physics and suits various requirements for a practical system. Secondly, there is the diversity of usable materials and functions. The progress of molecular material engineering has made it possible to synthesize polymers with performances similar to or better than their inorganic counterparts. By introducing functional groups to unsaturated monomer or oligomer units in a molecular structure, or just by doping the functional polymers into known photopolymerizable materials, optical, electronic, magnetic, and mechanical functions can be imparted to devices.

2.Functional Micromachines and Microelectromechanical Systems and their Optical Actuating

A number of micro components have been fabricated by 2PP .These structures are good proof of the fabrication capability of 2PP technology. Even more complicated devices can be produced, which should be composed of two types of components classified according to their functions, static parts for support, connection or confinement, and movable parts. Both need precise shaping, positioning and jointing during photofabrication.

For movable components, an essential issue to address prior to fabrication is finding a suitable actuating mechanism. Appropriate electric, optical, thermal, magnetic, and chemical effects need to be found to achieve this end. Electrically controlling micro systems, the requirement of MEMS, is most desirable. However, there is a long way to go before introducing conductive polymer into structures and integrating polymer devices on an IC-contained semiconductor chip or developing polymer ICs. Optical force provides a simple solution, which is the currently most practical mechanism for actuating micro-nano-devices.

The technique of optical manipulation has been employed as a unique means of controlling micro-dynamics of small objects without physical contact since the pioneering works by Ashkin [31,32]

The laser irradiation pressure (gradient and scattering forces) forms the basis of light actuation of micromechanical devices, which falls into three categories: windmill rotation, rotating by photon angular momentum transfer, and push-pull due to 3D trapping. In the following sections, we will describe how these optical powering approaches have been or will be applied for driving micro-machines.

For example ,windmills rotate when facing wind, a phenomenon known since ancient times. It is not surprising that similar rotational phenomena have been frequently observed in laser-trapped particles. The rotational torque arises from the axial irradiation force and from the asymmetrical or rotation-symmetrical shape of the particles. The rotation rate is proportional to the trapping laser's power, and is related to the shape of the objects and the viscous drag from the ambient medium.

In a micro-machine, it is important to design a device structure of helical shape and of proper rotation symmetry so that the structure could be fixed (trapped) at a suitable position and with the desired orientation, for high stability and for minimizing the friction between the rotating parts and its axle (if there is one). The translation momentum from the "photon wind' 'needs to be efficiently converted to the spinning momentum of the object. A number of micro-components satisfying the above requirements have been produced by various micro-fabrication technologies [34-36].

3 Mechanics of Two-Photon Polymerized Nanodevices

Like numerous electronic devices, such as personal computers and cellular phones, that have gained cost advantage from integrating most of their functions onto a single chip, mechanical micro-nanodevices and their integrated systems are expected to spur the next revolution in the manufacturing industry .It is already a well known principle in the aircraft manufacturing industry that real-size systems that are proportionally scaled up

from designed models don't work. This is because the surface area and mass (or volume) of an object do not proportionally increase with dimensions and they follow different laws (square and cubic laws respectively). The same principle applies when the size of devices are scaled down to micro nanometer sizes. For example, if the feature size of a device is reduced from millimetres to nanometers, the surface-to mass ratio increases by 10^6 times.

Therefore, in the nano realm, mass and inertia are no longer important, while physical, mechanical and electric characteristics such as stress and tension, thermal transfer, phase transition, fluid phenomena, and achievable field strength abide by rules much different from current experience and would dominate .

2PP has been recognized as an important method for producing micromechanical and MEMS devices. It provides a good opportunity to explore nano-device mechanics. Sun et al. [13, 37] fabricated a nano-spring using this technology. The laser system for TPA photopolymerization, with a wavelength tuned to 820 nm, was used for the laser trapping. When the laser focus was carefully adjusted , the bead was found to be three-dimensionally trapped and able to be freely manipulated. The spring was pulled by moving the trapped bead, and then it was released by blocking the laser, initiating an oscillation. The spring was observed to be prolonged from its original length, and restored to its original state after the laser was turned off .Elongations of up to 7 μm over many cycles didn't cause any elasticity failure, as evidenced by the fact that the spring always returned to its original length.

B Three Photon Absorption and Polymerization

2.6 Three Photon Polymerization

3PP initiated through the non linear process of three-photon absorption of a photoinitiator , and induces several chemical reactions between starter molecules and monomers in a transparent resin . The probability of three-photon absorption by the photoinitiator is proportional to P^3, where P is the laser pulse energy and 3 is the number of photons involved in the process.[38]

Thus, under tight-focusing conditions, three-photon absorption occurs only at the focal point and polymer is only formed within a volume on the order of λ^3, where λ is the laser wavelength.[39] By scanning the focal point in the x, y, and z directions throughout the sample, the desired pattern can be formed.[50]

Cross section of Three Photon Absorption

The three photon absorption is a nonlinear process and requires high intensities 10^{30} photon/cm^2sec .Just as the two photon absorption cross section is proportional to $Im(X^{(3)})$ the three photon absorption cross section is proportional to $Im(X^{(5)})$. The analysis of three photon absorption is an extension of three photon absorption case .If we include three photon absorption equation 17 will be modified as

$$\frac{dI}{dz} = -(a_1 I + a_2 I^2 + a_3 I^3) \qquad 1$$

where a_3 is the three photon absorption coefficient and is related to the imaginary part of $X^{(5)}$ .If we assume negligible linear and two photon absorption ,and a rectangular spatial and temporal profile the solution to this equation is

$$I(Z) = \frac{I_0}{\sqrt{1 + 2a_3 z I_0^2}} \qquad 2$$

The three photon absorption cross section σ_3 (cm^6s^2) is related to a_3 and the number density of the solute molecules N_0 by

$$(hv)^2 a_3 = \sigma_3 N_0 \qquad 3$$

The TPA cross section is related also with single photon absorption cross section .

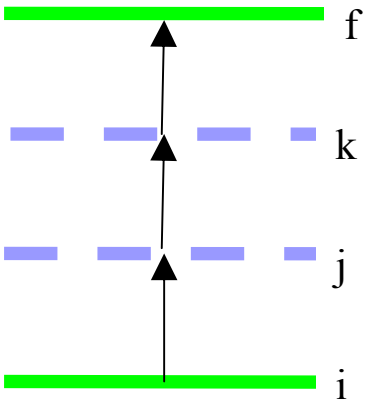

Fig 5Three layer system

$$\sigma_3 = \sigma_{ij}\sigma_{jk}\,\sigma_{kf}\,\tau_j\tau_k \qquad 4$$

where σ_{ij} is one photon cross section which is 10^{-16} cm^2 and τ can be calculated by Heisenberg principle and is 10^{-16}sec. So the TPA cross section is $\sigma_3 = 10^{-80}\,cm^6 s^2$.

2.7Applications

Three photon polymerization (3PP) of photosensitive materials allows one to fabricate complicated three-dimensional (3D) microstructures with sub-micron resolution . When laser is tightly focused into the volume of a liquid resin (which is transparent in the infrared), can initiate 3PP and produce structures with sub-micrometer resolution. The desired micro-structures are created by shifting the laser focus along three dimensions using a piezo-stage .The non irradiated resin is removed using an alcohol solution after processing .

However, while layer-by-layer lithographic techniques allow precise control over defect fabrication, they are tedious, expensive, and limited to structures consisting of a finite number of layers.Three - photon polymerization is unique in its ability to fabricate intricate sub-micrometer 3D features because of the nonlinear sensitivity of the photoinitiation step to photon flux.

Three-photon polymerization has been reported as a promising technique for the fabrication of intricate 3D objects with sub-micrometer feature sizes, including 3D woodpile structures,[38-40,42,43]] micro-machines,[44] photonic crystals [45,46] ,microrotors driven by laser tweezers [47] , mechanical devices [48,49]

C Future Prospects

Two and three photon photopolymerization, as an important method of multi-photon laser micro-nanofabrication, is expected to play an essential role in producing polymer-based optoelectronic and MEMS devices. A lot of work has been done along this line as previously reviewed .Future research in materials, optics and fabrication of functional devices are needed to further its use in diverse scientific research fields and industrial applications.

From a materials point of view, synthesis of two-photon chromophores with even higher two-photon cross-sections is required, so that photopolymerization may be induced by less expensive picosecond, nanosecond and even CW lasers for commercial applications. Also the high σ_2 materials would enable polymerization simultaneously from multi-beam split out of one output of a laser for batch production. Also desired is the use of copolymerization of functional molecules and resins, or doping of other functional components like nano-crystals into resins, so that particular functions could be imparted to polymerized devices.

From the optical standpoint, tailoring the point spread function to produce a spherical voxel shape is advantageous for precise 3D prototyping. Another important line of work is finding suitable mechanisms to construct a parallel production system. This may be accomplished by a diffraction beam splitter or by a micro-lens array. The latter is preferable because (i) foci number increases simply by expanding the area of a lens array since a single micro lens occupies a fixed size, for example, 250 μm diameter (ii) no further focusing is needed since each beamlet is naturally focused after passing through the array. Measures should be taken to ensure a uniform power distribution for sensitive control of polymerization from each beam. Without the capability of batch production, the cost of single-beam writing would severely hinder the versatile industrial use of the technology.

Chapter 3 Acoustic Biosensors

3.1 History of Surface Acoustic Wave Device

Biosensor is a system that can measure physicochemical changes that take place when a biological molecule reacts with another biological molecule . This system consists of three parts: a) the transducer that measures the physicochemical change and it can be acoustic, optical or electric, b) the biological material that is immobilized on the surface of the sensor and it reacts with some molecule added in solution and c) the electronic part that receives the signal from transducer and records it using the appropriate software.(fig1)

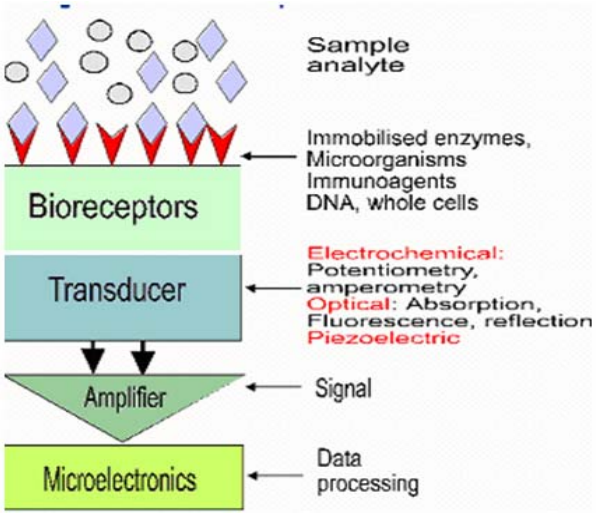

fig 1 Principle of operation for biosensor

The use of the acoustic waves in sensor technology relies on the phenomenon known as piezoelectricity which was discovered in 1880 by Curie brothers. In their classical experiments, plates of various crystals (including quartz) were subjected to applied pressure, the resulting electrical effect being recorded on an electrometer by means of tin foil electrodes. Curie brothers were able to verify that the application of electrical energy can result in crystal mechanical deformation.

In 1885 Lord Rayleigh confirmed the existence of elastic vibrations on the surface of solid materials. Ultrasonic and piezoelectric resonators [51] were discovered after some years. Other type of bulk wave devices based on Love, Lamp or Stonely

waves became important in the 1950s in the development of dispersive delay lines for radar and sonar applications. The combined usage of piezoelectricity with microelectronics began in the 1960s, when White and Voltmer showed that photolithographic techniques could be employed to deposit interdigital transducers (IDTs) on piezoelectric substrates to directly excite and couple to elastic surface waves [52] .

The acoustic wave can propagate in a quartz biosensor with a variety of ways. There are two main categories of biosensors which use two different types of waves; the SAW bionsensors, which use surface acoustic waves (SAW waves) and the BAW biosensors, which use bulk acoustic waves (BAW-waves) [53]. In the SAW biosensors, the acoustic wave propagates on the surface of sensor and it is the unique acoustic biosensor that can be used for the transaction of experiments in a liquid medium, as the wave propagates horizontally on its surface. In the case of the BAW sensor, the acoustic wave propagates through bulk volume of the piezoelectric material (Cady, 1924).The biosensors that function with SAW waves are much more sensitive than those that function with BAW waves, as they use higher frequencies in order to detect changes of mass on the surface of sensor (Gizeli et al., 1992a). The first description of a SAW chemical sensor, which was published by Wihtjen and Dessy in 1979, involved deposition of a sorptive film on the surface of the device[54,55]. The most widely used acoustic biosensor is the shear horizontal surface acoustic wave device (sh-SAW sensor) .

3.2 Surface Acoustic Wave Sensor based on Love waves

Surface Acoustic Wave devices are favoured for their use in chemical sensing applications because of their small size, low cost, high sensitivity and reliability . The shift in phase velocity and attenuation is measured by recording the frequency and insertion loss of SAW devices, respectively. Various effects , including mass loading, viscoelastic (elastic) effect loading and acousto-electric coupling contribute to SAW liquid response. In addition, the SAW device has been employed as a pressure sensor, chemical sensor [56,57], gas sensor and biosensor[58,59]. Fig 2 shows the frequency spectrum of an acoustic and an electromagnetic interdigital sensor.

The operating range of SAW sensors is from below 10MHz to slightly above 1000MHz .

Acoustic sensors can be used in extreme environments as liquid helium temperatures, vacuum and in complex conditions as those that they prevail in biological materials systems. Today, certain sensors are available commercially, while other remain experimental tools.

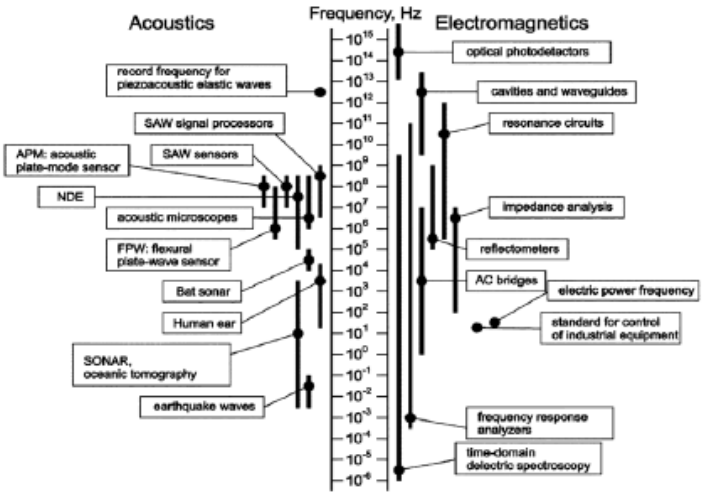

Fig 2 Frequency spectrum of acoustic and electromagnetic interdigital sensors

For our experiments a 108 MHz quartz device is used. This is fabricated on a 0.5 mm thick piezoelectric quartz crystal, more specifically a rotated Y-cut (42.5) quartz with propagation 90 deg with respect to the x-axis. The interdigital transducers (IDTs) comprise of 10/200-nm thick chromium/gold electrode and consisted of 80 pairs of split fingers with a periodicity of 45 μm. Fig 3

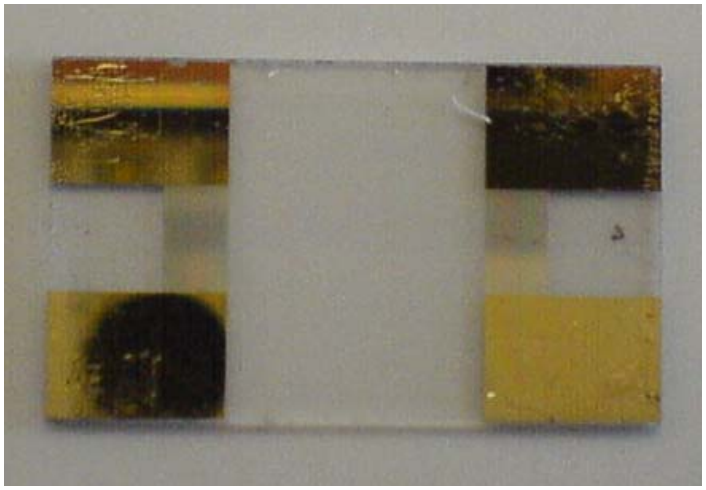

Fig 3 Acoustic Biosensor

3.3Characteristics of Acoustic Sensors and measurements

3.3.1 Fields in elastic materials

The elastic properties of a solid are mathematically described by the relation between stress and strain. When applying stress to a body, its deformation will be approximately linear as long as the applied stress is small enough. For larger stresses the strain response to the stress will become nonlinear but will still be elastic, which means that the body returns to its original shape as soon as the impressed stresses return to zero. For even higher stresses we enter the range of plastic deformation where the original shape of the body is not recovered for zero stresses. The displacement field then depends on the history and phenomena such as hysteresis can occur. Finally, for very high stresses cracks will occur and the fracture point is reached.

Consider a cube of solid material as shown in Figure 5 . Note that the number 1, 2, and 3 label the x, y, and z directions, respectively, and that the possible stresses are denoted as T_{ij} . The first subscript denotes the face on which the stress acts, and the second the direction of stress on the face. There is an array of nine stresses located in space, which is represented by the stress tensor [60]

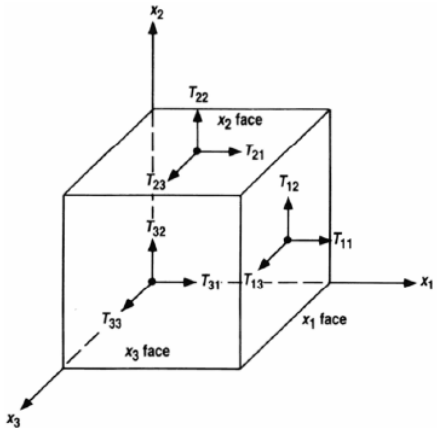

Fig 5 Stresses at points in space

$$T_{ij} = \begin{bmatrix} T_{11} & T_{12} & T_{13} \\ T_{21} & T_{22} & T_{23} \\ T_{31} & T_{32} & T_{33} \end{bmatrix} \qquad 1$$

The tensor must be symmetric (due to the conservation of angular momentum at each point), that is, $T_{ij} = T_{ji}$ and, therefore there are actually six independent components of the tensor. A second-rank tensor is termed because it possesses two subscripts. The application of stress on a viscoelastic medium causes a strain which is represented by the strain tensor:[61]

$$S_{ij} = \frac{1}{2}\left(u_{ij} + u_{ji}\right) \qquad 2$$

Where u_{ij} and u_{ji} are the displacements . For acoustic field problems we are mostly faced with very small displacement amplitudes, allowing for the assumption that we are operating in the linear range.

As it was the case for the stress tensor, due to symmetry, Equation 2 contains nine dependent variables. Now, the relation between stress and strain is expressed as follow:

$$T_{ij} = c_{ijkl} S_{kl} + n_{ijkl} \dot{S}_{kl} \qquad 3$$

This well-known equation describes, in its more general form, Hooke's law for a viscoelastic medium. The coefficients c_{ijkl} and n_{ijkl} are, respectively, the fourth-rank elastic coefficient tensor and the fourth-rank viscoelastic coefficient tensor. For time-varying fields, the presence of loss mechanisms will lead to imaginary parts for the elastic constants when using the concept of a complex harmonic time dependence exp (jωt). The material tensor c consists of 3^4=81 coefficients, which are not independent of each other. As the strain tensor and the stress tensor are both symmetric, the following symmetry conditions for the stiffness tensor can be obtained

$$\begin{aligned} c_{ijkl} &= c_{jikl} = c_{ijlk} = c_{jilk} \\ n_{ijkl} &= n_{jikl} = n_{ijlk} = n_{jilk} \end{aligned} \qquad 4$$

This reduces the number of independent coefficients from 81 to 36 (considering fundamental thermodynamic properties, the number of independent coefficients can be further reduced to 21 .

3.3.2 Fields in piezoelectric materials

So far we have only discussed purely elastic media. In addition to the effects described above, piezoelectric media become electrically polarized when they are strained. This polarization can be explained by the displacements of the atoms in the solid which produce microscopic electrical dipoles. For certain crystal classes these microscopic dipole moments may add up to a macroscopic polarization. The effect is (to the first order) linear, which means that the polarization changes sign when the strain is reversed. This behaviour is called the direct piezoelectric effect, which is always accompanied by the inverse piezoelectric effect corresponding to a deformation of the solid when an electric field is applied.

The effect of piezoelectricity is restricted to certain crystal classes. A very simple precondition for a piezoelectric crystal is that it must not have a centre of symmetry. To show this, imagine a piezoelectric crystal with a centre of symmetry and a particular impressed stress distribution creating an electric field strength in some direction. The inversion of the crystal and the stresses through the centre of symmetry should yield a field strength in the reverse direction. However, since the stress is centrosymmetric (which follows from the equilibrium of a volume element), the situation is the same as before and hence a centrosymmetric crystal cannot be piezoelectric. Note that this is only a necessary condition, actually one out of the 21 crystal classes being not centrosymmetric does not show the piezoelectric effect

Piezoelectricity is a coupling between the mechanical and electrical behaviours of a material. In other words, when a piezoelectric material is squeezed, an electric charge collects on its surface. Conversely, when a piezoelectric material is subjected to a voltage drop, it mechanically deforms.

3.3.2.aPiezoelectric Constitutive Relations

A principle , which relates stress to strain ,is known as constitutive relation , and can be generalized to three- dimensional piezoelectric materials. It is arised if we couple Maxwell ‘s laws of

electromagnetism with the fundamental and equations of materials .The coupling between electric field and strain is given by the electromagnetic constitutive relations :

$$T_{ij} = c^{E}_{ijkl} S_{kl} - e_{ijk} E_k + n_{ijkl} \dot{S}_{kl}$$

$$D_i = \varepsilon^{S}_{ik} E_k + e_{ikl} S_{kl} \qquad 5$$

where E_k is the electric field , S is the strain, T is the stress e_{ikl} is the piezoelectric stress tensor, with units charge/length^2 , D_I are the electrical displacement components , ε_{ik} are the dielectric strain tensor (6 values) ,and c_{ij} are the elastic stiffness constants .In these equations ,we discuss the sum over the repeated indices is assumed . The piezoelectric stress matrix is a third rank tensor ,and 18 piezoelectric constants are necessary to characterize a piezoelectric material. The form of e_{IJ} for various crystal classes is shown in table 2.3.The piezoelectric stress coefficient e_{ikl} is symmetric with respect to the indices l and k, while ε_{ik} is symmetric with respect to the indices i and k.

Material	Symmetry Class	e_{x1}	e_{x4}	e_{x5}	e_{y2}	e_{z1}	e_{z3}
Gallium Arsenide	Trig 3m		0.154				
Lithium Niobate	Trig 32			3.7	2.5	0.2	1.3
Quartz	Hex 6mm	0.171	-0.436				
Zinc Oxide	Cub 43m			-0.48		-0.573	1.32

Table1 Piezoelectric Stress Constants.

3.3.2.bWave equation for unbounded piezoelectric materials

From the piezoelectric constitutive relations it is a simple matter to derive the wave equation for piezoelectric media. The piezoelectric wave equation is typically written in terms of the displacement u_i coupled with an electrical potential Φ .

$$\sum_{j,k,l=1}^{3} c_{ijkl} \frac{\partial^2 u_l}{\partial x_k \partial x_j} + \sum_{j,k=1}^{3} e_{ijk} \frac{\partial^2 \Phi}{\partial x_k \partial x_j} = \rho \frac{\partial^2 u_i}{\partial t^2} \qquad 6$$

The second term may be considered as a source term responsible for the generation of an acoustic wave by an applied , time varying electrical potential. The equation 6 represents three equations of four unknowns u_1,u_2,u_3 and Φ. A fourth equation may be obtained from eq 7 for an unrestrained crystal at its surfaces (T=0) and with no free charges $(\nabla \bullet D = 0)$

$$\sum_{j=1}^{6} c_{ij} S_j = \sum_{j=1}^{3} e_{ij} E_j \qquad 7$$

So the equation 6 will be

$$\sum_{j,k,l=1}^{3} e_{jkl} \frac{\partial^2 u_l}{\partial x_k \partial x_i} - \sum_{i,k=1}^{3} \varepsilon_{ik} \frac{\partial^2 \Phi}{\partial x_k \partial x_i} = 0 \qquad 8$$

The above equation shows the effect of coupling between displacement and potential in piezoelectric plane materials.

3.3.3 SAW Excitation and Detection

A surface acoustic wave is excited on a piezoelectric crystal using an interdigital transducer (IDT). The principle of IDTs was first described by White and Voltmer [62].Application of a voltage between alternately connected electrodes imposes a periodic electric field to be imposed to the crystal. When an alternatie voltage is applied , a periodic strain field is generated in the

piezoelectric crystal . Thus, an acoustic wave perpendicular to the finger direction is excited by each finger pair. If multiple finger pairs exist, interference occurs yielding to a maximum SAW magnitude if

$$f_n = \frac{2n+1}{\lambda} v \quad , \; n \in 0,1,2,..... \qquad 1$$

where f is the excitation frequency and v is the acoustic wave velocity of the particular mode.

The transducer operates most efficiently when the saw wavelength λ matches with the transducer periodicity d. This occurs when the transducer is excited at the characteristic frequency defined by

$$f_0 = \frac{v_0}{d} \qquad 2$$

where v_0 is the saw propagation velocity

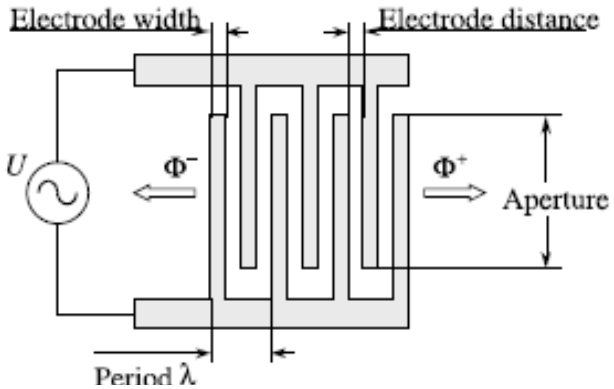

fig 6 Interdigital transducer (IDT) for the excitation of surface acoustic waves.

As we saw in previews paragraphs propagation of a mechanical wave in piezoelectric medium is accompanied by an associated wave potential Φ .When the wave is incident on a receiving transducer , this potential induces a current flow in each transducer electrode. These currents are combined to produce a current flow in the external detection cirquit.

The fundamental characteristic of an IDT is its frequency behaviour. An exact description considering the complicated electrical and mechanical boundary conditions is difficult and generally requires the utilization of numerical approaches.

3.3.4 Interdigital transducer frequency response

Each transducer finger may be considered to be a discrete source for the generation of the surface waves in a piezoelectric medium because the piezoelectrically generated stress varies with position near each transducer finger. A simple transfer function relates the continuous wave (CW) voltage V_1 applied to a finger and the electrical potential associated with the waves that propagate in each direction

$$\Phi^{\pm} = \mu_S V_1 \qquad 1$$

where μ_S is the substrate-dependent constant ,and Φ^+ is associated with the rightward propagating SAW ,while Φ^- is a leftward propagating SAW .The parameter μ_S is frequency independent and the frequency response of the transducer arises mainly due to the interference between finger contributions . fig 7

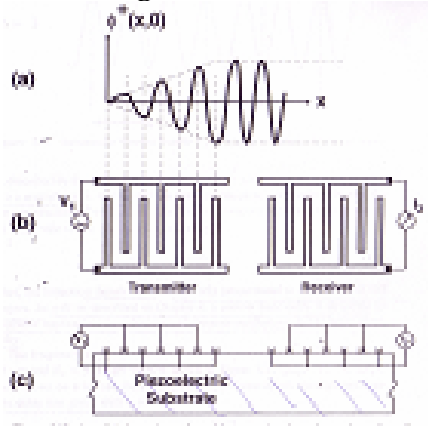

fig 7 Interdigitated transducer on the surface of quartz a)SAW electrical potential b) plan view c)side view

When an array of fingers is excited , as occurs with an interdigital transducer (IDT) the wave potential for a rightward wave Φ^+ evaluated at position z is a vector sum of the contributions from each finger.

$$\Phi^{+}(z) = \mu_S \sum_{n=0}^{N_f - 1} V_n e^{ik(z - z_n)} \qquad 2$$

where z_n the position of the n^{th} finger excited with voltage V_n and N_f is the total number of fingers.

For N_f identical fingers spaced periodically with spaced d and excited with alternating voltages $V_0(-1)^n$ the equation 2 will be for z=0

$$\Phi^+(0) = \mu_S V_0 \sum_{n=0}^{N_f-1} (-1)^n e^{-inkd/2} \qquad 3$$

This sum is a geometric series whose elements become unity , and add constructively , when kd/2=mπ where m is an odd integer. This condition defines the relationship between saw wavelength λ and transducer periodicity d. The IDT excites odd harmonics at odd multiples of the synchronous frequency.(fig 8)

$$f_m = mf_0 \qquad 4$$

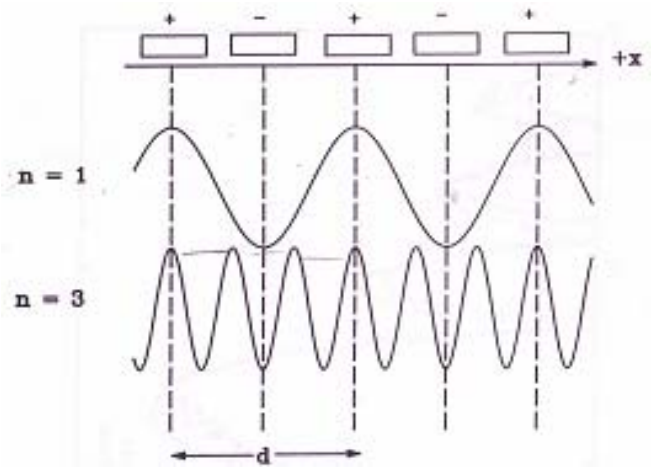

Fig 8 Relation between transducer periodicity and excited waves

Moving away from the synchronous frequency, the addition odd components from individual fingers become incoherent, giving rise to individual response.

$$\left|\Phi^+(f)\right| = \left|\frac{Sin(X)}{X}\right| \qquad 5$$

where

$$X = \frac{N_f \pi (f - f_0)}{2 f_0} \qquad 6$$

The wave equation as a function of the detuning parameter X is shown in fig 9. We can see that when X is a multiple of π , Φ^+ is zero a result of complete cancellation between finger contributions. The transducer bandwidth B between the first nulls on either side of the characteristic frequency is inversely proportional to the number of IDT fingers.

$$B = \frac{4}{N_f} \qquad 7$$

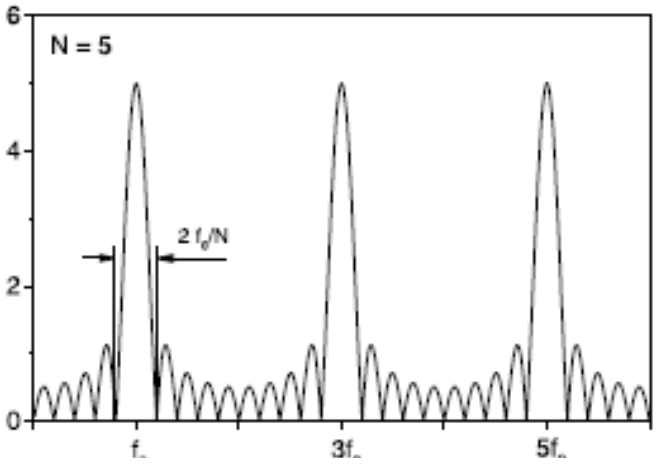

fig 9 Response of the $|\Phi|$ of a simple IDT as a function of the frequency.

A narrow bandwidth is desirable for oscillator applications in order to avoid spurious oscillations and to improve stability.

3.3.5 Delay line phase shift

One of the simplest and best known microacoustic structures is the delay line shown in Figure 10. The transducer IDT1 serves as the input for an electric radiofrequency (RF) signal which is transformed by means of the inverse piezoelectric effect into an acoustic wave travelling to the output transducer IDT2. Here, a re-transformation takes place back into the electrical domain. Hence the electrical signal experiences a delay τ because the acoustic wave is five orders of magnitude slower than the velocity of light:

$$\tau = \frac{D}{v} \qquad 8$$

where D is the centre-to-centre distance of the device and v is the

mean acoustic wave velocity. The basic idea is to define the transfer function as H(f)

$$H(f) = E(f,n)A(f) \quad 9$$

where E(f,n) is the frequency response of a single electrode .It depends mainly on the transducer geometry .A(f) represents the Fourier transform of the spatial voltage sequence of the actual IDT configuration . If no transmission loss occurs, the delay line transfer function H_{DL}(f) can be written as

$$H_{DL}(f) = H_1(f)H_2(f)e^{-j2\pi f\tau} \quad 10$$

with the transfer functions H_1(f) and H_2(f) of IDT1 and IDT2, respectively . The magnitude of the transfer function depends on the IDT characteristics, whereas D determines the phase φ:

$$\varphi = -2\pi\frac{D}{v}(f - f_0) \quad 11$$

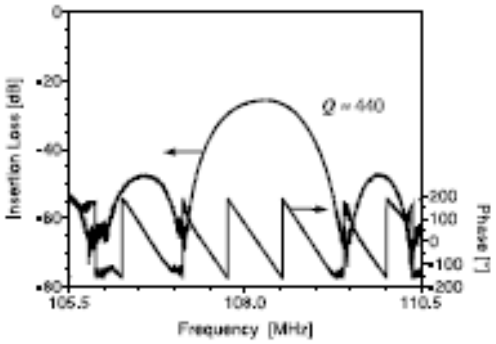

fig 10 Typical frequency characteristics of the basic microacoustic structures acoustic delay line.

3.3.6 PMMA as waveguide

PMMA is a polymer which is the guiding layer for the acoustic waves and is used because their very low shear acoustic velocity V_{pmma} = 1100 m s^{-1}, as compared to that of quartz V_{quartz} = 4950 m s^{-1} , (ρ=2,2 g/cm^3),results to a high energy confinement on the device surface. In addition, polymer layers have several practical advantages, because they can be formed on the device surface and subsequently removed by using relatively simple techniques.

Another critical parameter in designing a waveguide sensor is the thickness of the guiding layer because it affects the distribution of the power flow between the quartz and the polymer. Figure 11 gives a schematic representation of the variation in the power flow as a function of the over-layer thickness for the first mode of operation. When the thickness of the over-layer is much smaller than the wavelength, λ, most of the energy is located in the quartz substrate, and the Love wave propagates with a velocity, V_{Love}, that is very close to V_{quartz}. When thicker layers are applied, but are still of a thickness smaller than λ, the energy is concentrated in the over-layer and the velocity of the Love wave tends toward V_{layer}.

Between these two limits, the energy progressively transits from the quartz substrate into the layer and the velocity V_{Love} varies between V_{quartz} and V_{layer} .Finally, in addition to the energy distribution, the particle displacement on the surface of the polymer layer increases with increasing the over-layer thickness, which results in structures which are more sensitive to surface perturbations.[63]

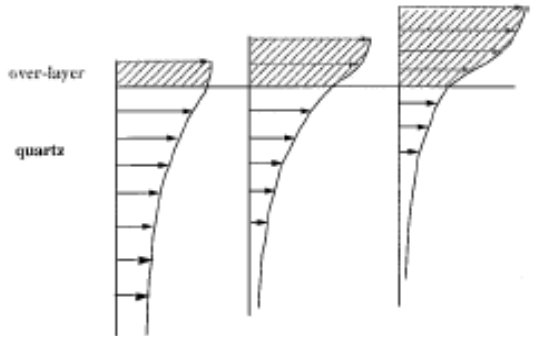

fig 11 Schematic representation of the power flow in the polymer over-layer and the quartz substrate as a function of the over-layer thickness.

3.3.7 Love waves propagation in a half-space solid

In 1911, Love discovers the Love wave, which is a shear-horizontal type of wave propagating in a guiding solid layer(PMMA) on top of a half-space solid as shown in Fig.12 . It is best known for applications in liquid sensing or sensing under liquid phases due to its small wave attenuation and energy loss into the adjacent liquid.

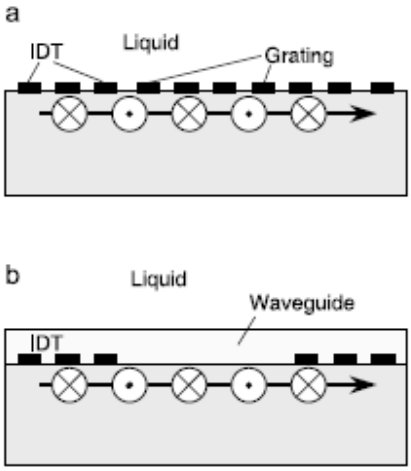

fig12 Surface transverse wave sensor (a) and Love wave sensor (b).

3.3.7 aMass loading effect

When vapour is sorbed in the sensitive layer, the resulting mass increase leads to a wave perturbation, this phenomenon is called mass loading effect. The effect of a thin-mass layer deposited on the surface of a Love wave device is the changing of the frequency or velocity of the wave. The most useful way to describe quantitatively the effect of mass loading is by using the sensitivity formula S_m, which is defined as the fractional change of the frequency of the acoustic wave, Δf, as a result of mass loading, divided by the operating frequency, f_o, and the deposited mass per unit area ($h\rho$). By definition, mass deposition refers to a layer with a thickness that is negligible as compared to λ_{Love} and, thus, cannot act as a waveguide layer.

$$S_m = \frac{1}{f} \lim_{h->0} \frac{\Delta f}{h\rho} \qquad 1$$

Generally, the most useful way to describe quantitatively the effect of mass loading is by using the sensitivity formula S_m, which is the fractional change in a parameter of the acoustic wave as a result of mass loading divided by the value of the same parameter before mass loading, per deposited unit mass per unit area ($h\rho$). Experimentally, the most common measurement is either

frequency change Δf , due to a layer of material, density ρ and thickness h loading the surface of the device and, S_{fm} is defined as

$$S_m^u = \frac{\frac{\Delta\beta}{\beta}}{[h\rho]} = \frac{w\left|u_y\right|^2_{x=\frac{b}{2}}}{4\beta P} \qquad 3$$

where Δβ is the change in the propagation constant β due to a thin mass loading layer of thickness h and density ρ, ω is the angular frequency, $|u_y|$ is the magnitude of the y-component (and the only non-zero component) of the velocity in the waveguide layer of thickness b and P is the total acoustic power flow through the entire trilayer structure, i.e. quartz, waveguide and liquid. The total power flow in the tri-layer system is given by[64]

$$P = \mathrm{Re}\left\{\frac{1}{2}\int_{\substack{cross\\ section}} \beta(c - in)\cdot\left|u_y\right|^2 dS\right\} \qquad 4$$

This is achieved by assuming that the substrate and the fluid are semi-infinite layers, hence the conditions at boundaries other than the waveguide boundary will have a negligible effect on the wave through the waveguiding layer. The nature of the contact between the layers gives rise to the boundary conditions; nonslip conditions at the boundaries are assumed, implying that there will be a continuity of displacement and shear stress across the boundaries. Thus, the displacement due to the acoustic wave in the device may be expressed as three trial functions, one for each layer, which are connected by the non-slip boundary conditions. The form of the trial function is based on the geometry of the device, and is written below.

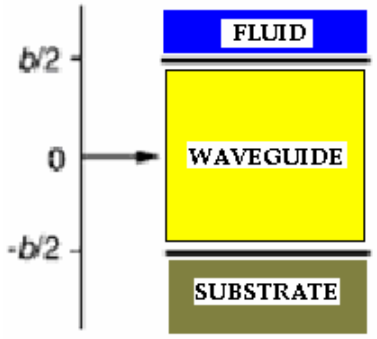

Fig 13 Geometry of the Love waveguide

$$u_y^{fluid} = Ae^{-(c+id)x}e^{i(wt-\beta z)} \quad (5)$$

$$u_y^{PMMA} = \left(Be^{ikx} + De^{-ikx}\right)e^{i(wt-\beta z)} \quad (6)$$

$$u_y^{sub} = Fe^{ax}e^{i(wt-\beta z)} \quad (7)$$

All the trial functions have a propagating-wave character through the $e^{i(\omega t-\beta z)}$ term while both the liquid and substrate functions decay as the wave moves further away from the waveguiding layer. The two solid layers are assumed to behave as ideal linear elastic materials and the liquid as a Newtonian fluid obeying the Navier–Stokes equation. By applying the boundary conditions to the trial functions, it is possible to derive a complex dispersion function F(kb), given by equation (8), along with the normalized displacement field equations, equations (9-11).

$$F(kb) = \tan(kb) - \frac{akc_{sub}c_{PMMA} + iknw(c+id)c_{PMMA}}{\left(k^2c^2{}_{PMMA} - ianw(c+id)c_{sub}\right)} \quad (8)$$

$$u_y^{fluid} = e^{(c+id)\left(\frac{b}{2}-x\right)}e^{i(wt-\beta z)}$$

$$u_y^{PMMA} = \left(\cos\left(k\left(x-\frac{b}{2}\right)\right) - \frac{inw(c+id)}{kc_{PMMA}}\sin\left(k\left(x-\frac{b}{2}\right)\right)\right)e^{i(wt-\beta z)}$$

$$u_y^{sub} = \left(\cos(kb) + \frac{inw(c+id)}{kc_{sub}}\sin(kb)\right)e^{i(wt-\beta z)}e^{\left(a\left(\frac{b}{2}+x\right)\right)} \quad (9\text{-}11)$$

By taking the time derivative of the displacement fields, equations (9-11), and then inserting them into the sensitivity formula, equation (3), it is possible to express the sensitivity of the device as a function of known parameters, i.e. the viscosity of the liquid layer η, the frequency of the wave f_o, the thickness b and the elasticity modulus c_{PMMA} of the waveguiding layer and unknown ones, such as the wavevector k, the propagation constant β, and constants c and d. However, the values for k and β may be

evaluated numerically, using a complex pair root finding technique called Muller's method .($c=u_{pmma}\rho$, u_{pmma}=1100m $^{-1}$ s ρ=1180kg/m^3 and $c=u_{sub}\rho'$, u_{sub}=4952m $^{-1}$ s,ρ'=2650 Kg/m^3)

This gives a more complicated expression , which is a function of the attenuation constant in the substrate a_{3X} and the wavevector in the overlayer k_{2x}.[65]

$$\frac{\frac{\Delta\beta}{\beta}}{[h\rho]} = \left(\frac{w}{\beta}\right)^2 \frac{1}{b}\left[c_{PMMA}\left[1+\sin c(2k_{2x}b)\right] + c_{sub}\frac{\cos^2(2k_{2x}b)}{a_{3x}b}\right]^{-1} m^2kg^{-1}, \qquad 12$$

To express the measured change of phase with the accumulated surface mass density it is necessary to modify (12) to a form (33), which includes the separation between transducer centres, D, and the velocity of the Love wave mode,u_{mode}

$$\frac{\Delta\Phi}{[h\rho]} = \left[360\bullet 10^{-5}\right]\frac{D}{u_{\text{mod}\,e}}\left(\frac{w}{2\pi}\right)\left[\frac{\frac{\Delta\beta}{\beta}}{[h\rho]}\right]\text{deg}/\mu gcm^{-2} \qquad 13$$

This equation is valid for a wide range overlayer materials from the modulus polymers to high modulus materials such as silica. For a PMMA thickness b=0.5128 μm and for D=0.009m the following parameters were calculated using 12,13

$$a_{3x}b = 2.428\bullet 10^{-3}$$
$$k_{2x}b = 3.1415\bullet 10^{-1}$$
$$V_{\text{mod}\,e} = 4950.44ms^{-1}$$
$$\Delta\beta/\beta[h\rho]^{-1} = 1.324m^2kg^{-1}$$
$$\Delta\Phi/[h\rho] = 5.494\,\text{deg}\left(\mu gcm^{-1}\right)$$

The piezoelectric and anisotropic nature of the substrate and the transduction process have been ignored. However, as they are not critical to the function of the sensing area, the model is expected to produce valid results.

3.3.7.b Viscous coupling

While shear waves show no interaction with ideal liquids, there is an interaction with viscous liquids. Assuming a non-slip boundary condition at the sensitive surface, a thin layer of liquid becomes entrained with the shear movement. Solution of the Navier -Stokes equation in the liquid indicates that the liquid undergoes a shear motion which decays rapidly with distance form the surface. The displacement near the solid/liquid interface, calculate for two different fluid viscosities at 158MHz is shown in Fig10 . From this Figure, it is apparent that the liquid layer entrained by the surface becomes thicker as the liquid viscosity increases.

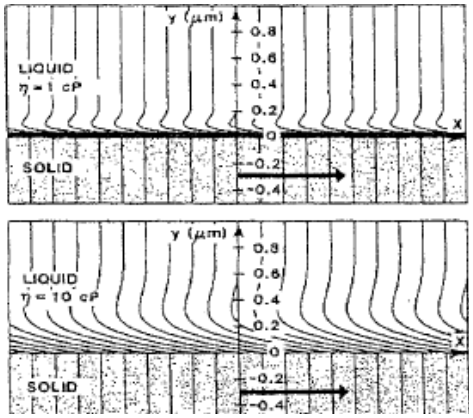

fig 14 Calculated velocity profiles at the solid/liquid interface showing entrainment of a thin liquid layer by the SH plate mode.

The characteristic decay length δ of this entrainment is given by [66]

$$\delta = \sqrt{\frac{2n}{\rho\omega}} \qquad 24$$

where n and ρ denote the viscosity and the mass density of the liquid, respectively, and ω is the angular frequency.

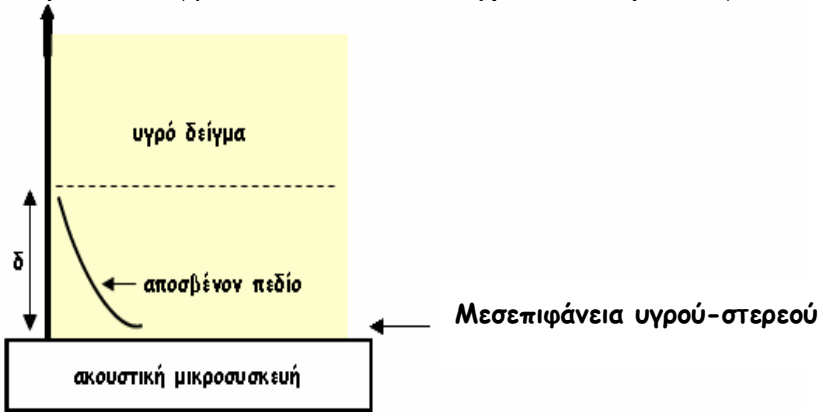

fig 15 Schematic representation of interface liquid solid where δ is the acoustic wave 's infiltration depth

From the equation 24 it is obvious that the changes in the frequency of acoustic wave influence the depth of infiltration . More analytically , increasing frequency leads to a decreasing in depth of infiltration so sensitivity is increased .

The viscous loading affects the Love wave in two ways. First, by the entrainment essentially represents a mass loading of the waveguide, which yields an according change in the wavenumber ,κ = 2π/λ (λ denotes the wavelength) of the wave. Secondly, the wave becomes damped due to the viscous losses in the liquid. These effects can be analysed using perturbation theory , which yields the following expression for the relative change of the complex propagation constant y (scaled to the unperturbed wavenumber κ) [67]

$$\frac{\Delta\gamma}{k} = \frac{\alpha + j\Delta k}{k} \approx \frac{1+j}{\sqrt{2}} S\sqrt{\omega n\rho} \qquad 25$$

The real and the imaginary parts of Δγ represent the induced damping α and the change in wavenumber Δκ, respectively. S stands for the device sensitivity [68], which describes the sensitivity of a Love wave with respect to surface mass loading. The wavenumber and the damping are related to th phase delay and the insertion attenuation of the love sensors respectively. S directly depends on the scaled overlayer thickness H/λ, which makes it a characteristic quantity depending on the geometry of a particular device, since the wavelength h at the centre frequency of the delay line is prescribed by the IDT period. S is furthermore related to the mass sensitivity S_m which gives the relative change of the wavenumber k due to a (infnritesimal) surface mass loading Δp:

$$S_m = S\omega \qquad \text{where} \quad S_m = \frac{1}{k}\frac{\Delta k}{\Delta\rho} \qquad 26$$

3.3.8 Theoretical of the phase shift

The changes of the velocity will be derived to the phase delay in an elastic half-space loaded with a fluid as shown in Fig.11, and the phase equations of loading without liquid and with liquid are as, respectively,

Phase of loading without liquid $$\Phi_0 = \frac{L}{\lambda} 2\pi \quad (27)$$

Phase of loading with liquid $$\Phi' = \left(\frac{L - d'}{\lambda} + \frac{d'}{\lambda'} \right) 2\pi \quad (28)$$

where L is the distance between the IDTs, d' is the area of liquid loading, λ and λ' are the wavelength of loading without liquid and with liquid respectively, and Φ_0 and Φ' are the phase of loading without and with liquid, respectively. The direct wave transmission form one IDT to another are considered in the derivations and are neglected other indirect multi-transmission or multi-reflection of acoustic waves from the edges.

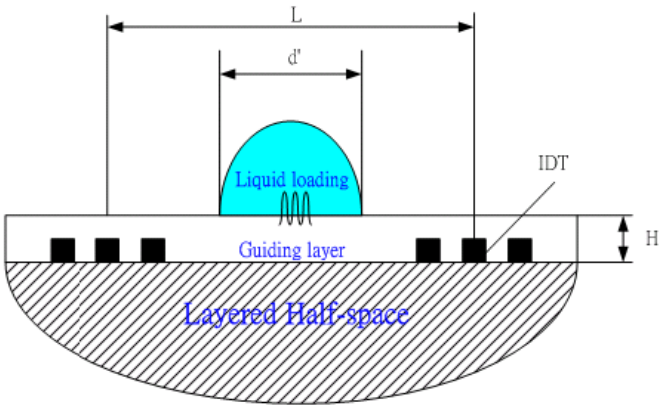

Fig16 An elastic half-space is under liquid loading

$$\frac{\Delta V}{V} = -\left(2\pi \frac{d'}{\lambda} \right) \Delta\Phi \quad (29)$$

The above equations is the relation between the fractional velocity change and phase delay with liquid loading. Where the V/ΔV is the fractional velocity change at the phenomenon of the change in perturbed and unperturbed surface with the liquid loading carrying SH waves. The ΔΦ is the phase shift with the liquid loading.

3.3.9 Electromechanical coupling coefficient K^2

The electromechanical coupling coefficient K^2 is a measure of the efficiency of a given piezoelectric in converting an applied electrical signal into mechanical energy associated with a surface acoustic wave. Here K^2 and SAW velocity u represent the two most

important practical material parameters used in SAW design. (table 1)

Material	Crystal Cut	SAW Axis	Velocity (m/s)	K^2 (%)	Temp. Coeff. (ppm/°C)	Capacitance/ Finger Pair/ Unit Length C_0 (pF/cm)	Application
Quartz	ST	X	3156	0.11	~0 near 25°C	0.55	Precision Oscillators, Temperature-Stable Narrowband Midloss IF Filters, Lowloss RF Filters
Lithium Niobate $LiNbO_3$	Y	Z	3488	4.5	94	4.6	Wideband Midloss IF Filter
$LiNbO_3$	Y128°	X	3992	5.3	75	5.0	Wideband Midloss IF filter
Bismuth Germanium Oxide $Bi_{12}GeO_{20}$	110	001	1681	1.4	120	-	Long Delay Line
Lithium Tantalate $LiTaO_3$	77.1° Rotated Y	Z'	3254	0.72	35	4.4	Oscillators Minimum Diffraction Cut
Gallium Arsenide GaAs	(100)	<110>	<2841	<0.06	35	-	Semiconductor IC Compatible

Table 1

For SAW wave propagation in piezoelectrics, it is shown that the electromechanical coupling coefficient K^2 can be defined in terms of piezoelectric coefficient e, elastic constant c and dielectric permittivity ε

$$K^2 = \frac{e^2}{c\varepsilon} \qquad 30$$

3.3.10 Saw acoustoelectric response

When a SAW propagates in a piezoelectric material ,it generates a layer of bound charge at the surface that accompanies the mechanical wave. This bound charge is the source of the wave potential Φ and also generates an evanescent electric field, shown in fig…

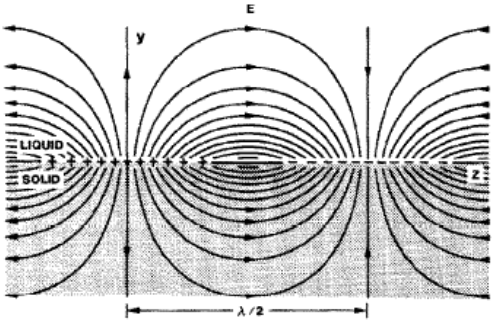

fig 17 Propagation of acoustic wave in a piezoelectric material generates an evanescent electric field that extends into the adjacent liquid ,coupling to ions and dipoles in solution.

When a conductive film is deposited onto the saw medium ,charge carriers in the film redistribute to compensate for the layer of bound charge generated by the passing surface wave. The current generated per area of surface I_0 is

$$I_0 = 2K^2 w\beta^2 (\varepsilon_0 + \varepsilon_S)P$$

where K^2 is the electromechanical coupling coefficient squared and ε_0 and ε_s liquid and substrate dielectric permitivities ,respectively ,β and P are the acoustic wave number and power density. The magnitude of acousto-electric response is proportional to K^2 so is thus substrate dependent. So sometimes acousto-electric response can be much greater than the mass loading effect.

3.3.11 Controlling the sensor Enviroment

Acoustic wave devices are sensitive to a large number of physical and chemical measurements. These include parameters such as temperature ,pressure ,acceleration ,stress ,and the adjacent medium' s density ,viscoelesatic properties and electrical conductivity .It is crucial the sensor environment to be carefully controlled in order to to eliminate the effects of sensor cross sensitivities.

a)Temperature Effects

Temperature has a direct effect on the operation of all acoustic wave devices .Ghanges in temperature are responsible for changes in the density of the substrate ,which changes the velocity of the acoustic wave . There are three main methods by which the effects on temperature on AW sensors be minimized 1)selection of low temperature coefficient materials. 2)incorporation of a temperature sensor and compensation circuitry or software and 3) active control of the sensor temperature .

b)Pressure effects

Ambient pressure can affect acoustic waves devices in two ways. Firstly it can hydrostatically compress the device ,resulting in small pertubations in the wave velocity and length of the AW path .Secondly it can affect the density of the fluid medium in contact with the device. In addition a pressure change can perturb the equilibrium concentration of sorbed species (e.g. water) on the sensor/coating surface.

c)Flow rate Effects

Flow conditions and geometry of the surface

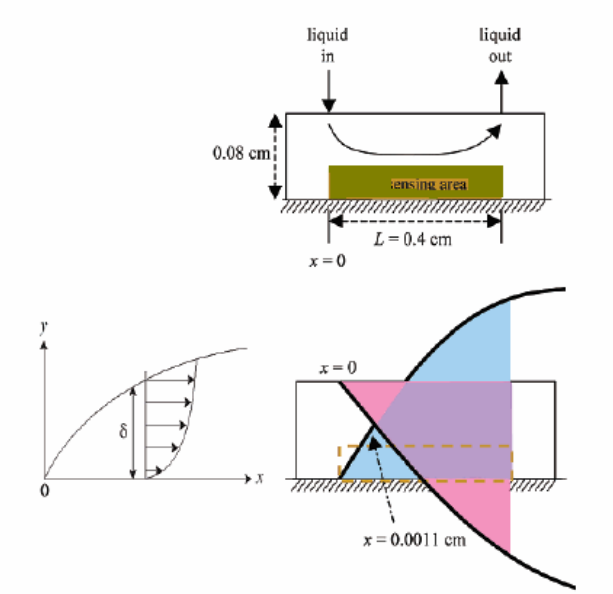

fig 7 Schematic of liquid flow cell with overlapping developing boundary layer schematic. Boundary layer shown for laminar flow in the middle of sensing area. δ is the boundary layer thickness. Drawing not to scale.

Analogously in flow situations, there is a thin static medium at surfaces called the "boundary" layer (Fig 7). In this layer, the velocity and concentration of a species changes from that in the bulk of the solution to that at the surface. Flow conditions and geometry of the surface strongly affect the thickness of this boundary layer, which correspondingly affects the mass-transfer resistance of a species from the bulk to the surface.

Mass transfer is sensitive to velocity in the flow direction, v_x (fig 7) , and for our geometry is simply the flow rate divided by the cross-sectional area. With flow rate at 40 µL/min and cross sectional area of 0.08 cmx0.391 cm, v_x was 0.021 cm/s. The Reynolds number (Re) in the flow direction is given by

$$\mathrm{Re}_x = \frac{\rho v_x x}{n}$$

where ρ is the density of flowing medium and n is the viscosity of flowing medium. At the end of the flow cell, with v_x = 0.021 cm/s, ρ=1.0 g/cm^3, n= 0.01 g/cm s, and L = 0.391 cm, Re_L =0.81. For such low Re, flow is laminar.[69]

Using the Blasius approximation, the thickness of the boundary layer for laminar flow, δ(x), at both boundaries at a certain distance x from the entrance of the flow is calculated:

$$\delta(x) = 1,72x\left(\mathrm{Re}_x^{-0,5}\right)$$

At the end of the flow cell, the boundary layer thickness, δ(L), is 0.75 cm. A simple approximation to estimate a lower limit of mass transfer is used: laminar flow at the same velocity over a flat plate (the case when there is no top boundary in the flow cell).

At low flow rates , and with the appropriate cell design , the flow over the sensor surface can be laminar .This may increase the apparent response time of the sensor because the vapour molecules will need additional time to diffuse through the boundary layer immediately above the coating. Turbulent flow, which is encountered at higher flow rates .Turbulent flow , which is encountered at higher flow rates can result in faster response since the boundary layer thickness is reduced.

3.4 Love wave device Advantages and Disadvantages

Because the acoustic energy is trapped near the micro-device's surface and it is not diffused in the device they are much more sensitive sensors toward to bulk wave (eg QCM)

Moreover SAW devices detect molecular interactions in real time. SAW devices operate in high frequencies so they are more sensitive in the reactions that happen on surface. When the device is made of lithium tantalate or lithium niobate this sensitivity is increased even more.

Since the detection happens only on the surface of the device , this means that that the behind part of the device can be connected in something else without problems with the signal. This does not happen with bulk wave devices (eg QCM) because the waves interact with the two surfaces.

A disadvantage is that the research based to acoustic devices is carried out finally only years and thus will need enough time fo using in a wide and potentially commercial scale (Tullier M., 2004)

Chapter 4 Materials and Methods

4.1.1ORMOCER polymer

ORMOCER stands for ORganically MOdified CERamic and it is a family of organic-inorganic hybrid polymers created by the Fraunhofer Gesellschaft (Fraunhofer-Institut fur Silicatforschung, Wiirzburg, Germany)[70]. Because of their physical and chemical properties which result from their hybrid nature inorganic–organic polymers have been developed and tested for evaluation in optical and electrical interconnection technology over the last decade [71]. The specific ORMOCER used in this work is a hybrid developed for optical applications so that shows high transparency in the visible and near infrared ranges. It consist s of an inorganic Si-O-Si backbone and the polymerizable functionality is introduced into the system by organic side chains R, e.g., (meth-) acryl groups.(Fig. 1). The optical and mechanical properties, that is, absorption and refractive index, are controlled by the other side chains such as methoxy (Me) and phenyl (Ph) groups.

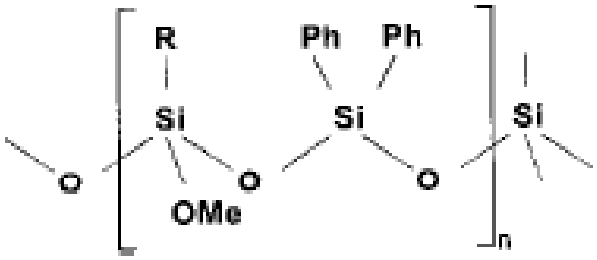

fig 1Chemical structure of ORMOCER polymers. Methoxy (Me) and phenyl (Ph) groups are linked to the inorganic Si-O backbone.

The light sensitivity of the ORMOCER-type hybrid polymers in combination with appropriate photoinitiators permits the photolithographic fabrication of optical microstructures. In the specific ORMOCER used in this work, initiation of the free-radical photopolymerization process is due to a photoinitiator Irgacure 369 (fig 2), which absorbs strongly in the UV wavelength range around 350 nm (fig 3).

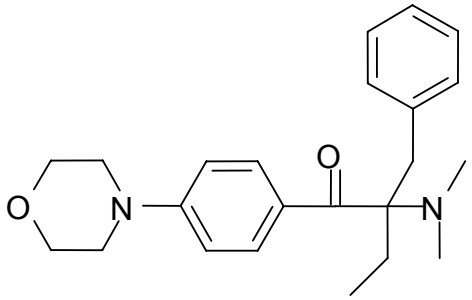

fig 2 Chemical structure of Irgacure 369

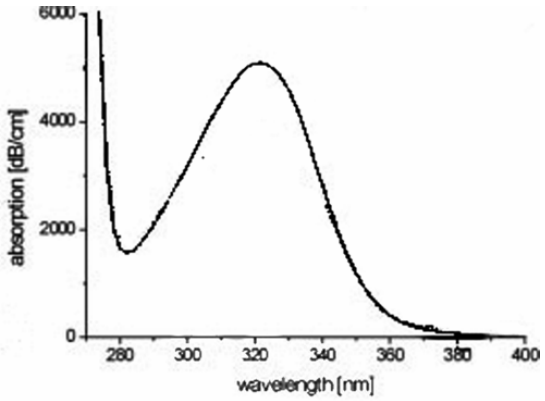

fig 3 Absorption spectrum of ORMOCER

4.1.2 Production of ORMOCER

The ORMOCER used in the worked is obtained prepared from Microresist (Germany). The preparation of the material is, however, straightforward and described below.

In order to either achieve a suitable inorganic–organic hybrid polymer, an inorganic backbone is established via poly condensation (alkoxylation) of diphenylsilanediol (P2) and 3-methacryloxypropyltrimethoxysilane (MEMO) referred to as ORMOCER I. Fig.4 shows the reaction scheme for the resin of ORMOCER_I which is used as the core material for optical waveguide applications, where P2 and MEMO react using a suitable catalyst at an elevated temperature.

$$RSi(OMe)_3 + R_2' Si(OH)_2 -> Polysiloxane + 2MeOH$$

where R is the methacrylic group and R_2' is the diphenyl.

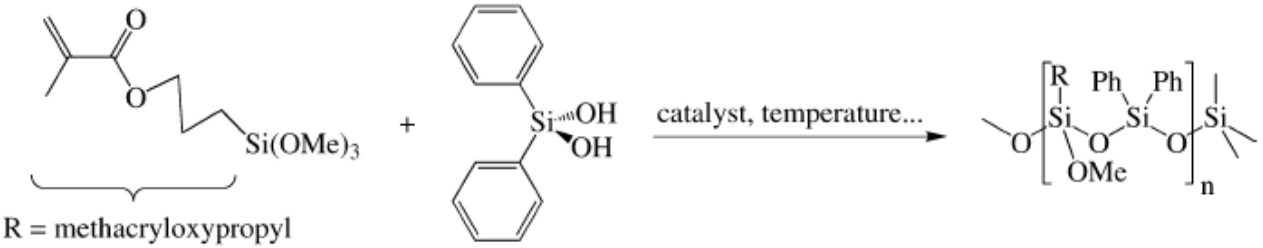

Fig4 Reaction Scheme of silane precursors of polysiloxane network used as polymer core material. ORMOCER I results after UV polymerization of the organic group R .

After this reaction, volatile products such as methanol (MeOH) are evaporated resulting in a viscous, storage-stable ORMOCER resins [72].

4.1.3 Polymerization of ORMOCER

The infra-red laser passes through the out of focus photosensitive resin with no absorption. Nonlinear absorption of laser pulses breaks chemical bonds on starter photoinitiator molecules within a small focal volume. The monomers react with with radicalized starter molecules to create radicalized polymolecules. Reactions are terminated when radicalized polymolecules react with one another. The main reaction series in three photon-induced polymerization is shown below

$$A \xrightarrow{3h\nu} A^*$$

$$A^* + M \longrightarrow A^* + M^* \qquad \text{Initiation}$$

$$M_n^* + M \longrightarrow M_{n+1}^* \qquad \text{Propagation}$$

$$M_n^* + M_m^* \longrightarrow M_{n+m} \qquad \text{Termination}$$

where A is photoinitiator, M is monomer and M^* is growing radical.

The self-organizing character of photosensitive polymers like ORMOCER arises from the change of the material density during the polymerization process. This density change corresponds to a change in the refractive index. This index change is permanent and

saturable. As long as oxygen is kept away, the nonlinear response is available directly after the illumination is started, when the first photons are absorbed by the photoinitiator . If the inhibition by oxygen is not avoided, a certain threshold energy E_{thres} has to be passed to get over the inhibition of the polymerization due to the interception of free radicals. Once the polymerization reaction is initiated, the refractive index grows fast at first .This is because all radicals find directly suitable reaction partners after short diffusion lengths in their closest neighbourhood. The index change passes then over into saturation with a slowly rising index, owning to the more and more limited mobility of monomer radicals in the partly cross-linked polymer matrix. In addition, the radicals have to diffuse longer to find available reaction partners. So the reaction velocity slows down, and the polymerization terminates. Besides the basic material properties, the nonlinear response depends strongly on a set of process parameters, such as the exposure intensity and the photoinitiator concentration and type.

4.1.4 General Properties of ORMOCER

Porosity and density

Classic ORMOCER is a dense material and its density lies between 1.1 and 1.6 g/cm^3 which is slightly above the range for organic polymers ,but well below the density of oxide materials($2.2g/cm^3$)

Mechanical and Thermal Properties

The inorganic structures of ORMOCERs are responsible for their high stiffness and hardness compared with organic polymers. Due to their transparency and easy of processing as lacquers ORMOCERs find widespread applications as coatings which exhibit high mechanical strength, hardness and abrasion resistance.

ORMOCER materials demonstrate mechanical properties that may vary from those of polymers to those of ceramics .For example ,Young's modulus values for ORMOCER materials may be adjusted between 1Mpa and 4000Mpa and thermal expansion

coefficients from 183 to $67x10^{-6}K^{-1}$ through the use of various precursors.

Optical and Electrical Properties

The high optical transparency of ORMOCERs is mainly due to their amorphous nature and their lack of structures absorbing light in the visible region ORMOCERs in their non-modified form are highly electrically insulating materials comparable to inorganic glasses and non-polar organic polymers. In addition, ORMOCERs adhere very well on most substrates such as (metallized) Si wafers, inorganic glasses and polymers

ORMOCER materials demonstrate optical transparency in the 1600nm range, refractive indices in the 1.47-1.56 range, and low optical losses in the near infrared range. These materials remain stable to 350°C in an oxygen atmosphere and exhibit duroplastic behaviour on heating.

ORMOCERs are highly insulating materials with bulk resistivities in the range of 10^{13}-$10^{16}\Omega$ cm. Therefore they show good passivation properties for electronic applications , due to their good adhesion to most of the interconnection materials and good barrier properties.[73] Their low dielectric constant makes them good candidates for interlayer dielectrics in electrical interconnection technology.

4.1.5 Applications of ORMOCER
Fabrication of 3D microstructures

Three photon polymerization (3PP) of photosensitive materials allows one to fabricate complicated three-dimensional (3D) microstructures . When they are tightly focused into the volume of a liquid resin (which is transparent in the infrared), femtosecond laser pulses can initiate 3PP and produce structures with submicrometer resolution. The desired microstuctures are created by shifting the laser focus along three dimensions using a piezo stage .The non irradiated resin is removed using a developer solution after processing.

Fabrication of photonic crystals

Liquid resins, like ORMOCER, are used to fabricate photonic crystals because they exhibit high transparency in the visible and near infrared ranges by means of 3PP .The rods have a thickness of 300nm and the woodpile structure possesses a photonic band gap in the near infrared spectral range. The central frequency of the bandgap can be tuned by varying the period of the crystal. 74,75

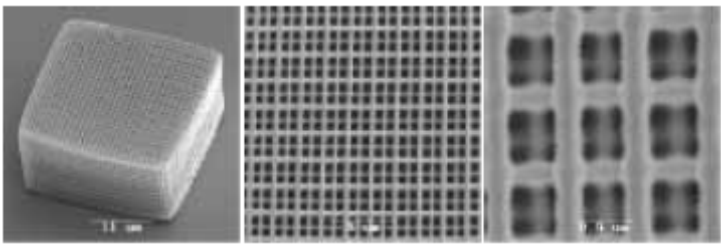

fig 5 SEM images of woodpile structures fabricated by means off 2PP in ORMOCERs

Medical applications

The precision of 2PP along with the unique properties of ORMOCER allow the development of microneedle arrays for drug delivery. Micron-scale needles can increase skin permeability and improve the transdermal delivery of macromolecules. Arrays of these needles could provide painless injections to people suffering from diabetes, blood clotting or other disorders .[86]

4.2 Eosin Y-sensitized acrylate composite

4.2.1Synthesis

The photo-polymerizable system used in this work is an acrylate-based photo-polymer and consists of three basic components: a sensitizer dye, an amine co-initiator and a multifunctional acrylate monomer. Pentaerythritol triacrylate (PETIA, Aldrich, Fig. 6a) forms the backbone of the polymer network. N-methyldiethanolamine (MDEA, Aldrich, Fig. 6b) is used as a co-initiator and Eosin Y (2-, 4-, 5-, 7-tetrabromo-fluorescein disodium salt, Aldrich, Fig. 6c) as sensitizer dye

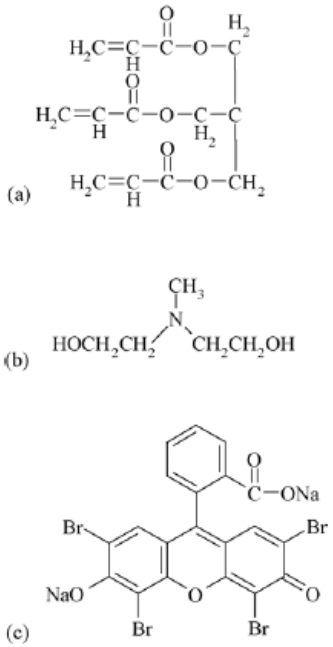

fig 6Molecular structures of the polymerisable materiala)PETIA b)MDEA c)Eosin Y

This system is particularly sensitive in the spectral region from 450 to 550 nm, where the two-photon absorption window for the 1028 nm laser lies. [82] Fig. 7 shows the normalized absorption spectrum of the PETIA/MDEA/Eosin Y composite, taken using a Cary 50 UV–vis/IR spectrometer. The material exhibited no absorption above 1000 nm and absorbed very strongly in the green spectral region, where the two-photon absorption window of the laser used lied. The absorption in the green was due to the addition of Eosin Y.

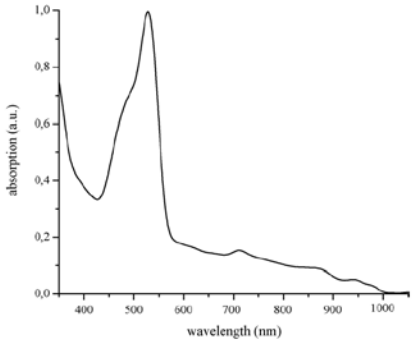

fig 7Absorption Spectrum of the polymerisable material

4.2.2Photopolymerization of Eosin Y

The two-photon polymerization reaction is initiated through a radical process. Two components are involved in radical formation: a dye capable of absorbing two-photons of infrared radiation and an amine that can be oxidized by the triplet state of the dye. Once the radicals trigger the polymerization, the monomers polymerize, developing into a three-dimensional network ,reach the gel point, and finally vitrify.

Step 1. Sensitization—formation of the triplet state of the dye

$$Dye \xrightarrow{2h\nu} {}^1Dye^* \longrightarrow {}^3Dye^*$$

Step 2. Radical formation—electron transfer from the amine to the dye, followed by proton transfer.

$${}^3Dye^* + RH \longrightarrow \left[{}^3Dye^{\bullet -} - - - RH^{\bullet +}\right]$$

(ion radical pair)

$$\left[{}^3Dye^{\bullet} - - - RH^{\bullet +}\right] \longrightarrow DyeH^{\bullet} + R^{\bullet}$$

Step 3. Initiation of the polymerization

$$R^{\bullet} + M \longrightarrow R + M^{\bullet}$$

Step 4. Propagation

$$RM_n^{\bullet} + M \longrightarrow RM_{n+1}^{\bullet}$$

Step 5. Termination

$$RM_n^{\bullet} + RM_p^{\bullet} \longrightarrow \begin{cases} RM_{n+p}R \\ RM_n + RM_p \end{cases}$$

The sensitivity of the system is characterized by the dose of energy it has to absorb to reach the gel point E_{gel}. The dose of the absorbed energy, before the polymerization itself occurs ,is called the threshold dose E_{th} and is related to the inhibition of polymerization by oxygen. Oxygen is known to prevent radical photopolymerization either through deactivation of the triplet state of the photoinitiator (precursor of radical species) or by trapping the initiating radicals themselves through peroxidation (Fig. 8)[83]

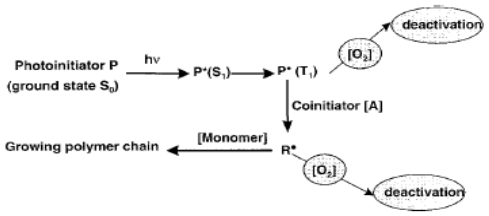

fig 8 Schematic representation of the effect of oxygen in light induced radical polymerization

At the end of the inhibition period, the absorbed energy is used to form the 3D polymer network; polymer chains start growing and the crosslinking reaction proceeds rapidly. Gel is not formed immediately and, at the onset of polymerization, the mechanical properties of the material are not strong enough to stand a washing off development . Mechanical resistance appears only when the dose received by the system is greater than E_{gel}.

The work reported in this paper has been obtained with the following reference formulation: Pentaerythritol triacrylate10 ml: N-methyldiethanolamine 0.1 ml: Eosin Y 10mg (dissolved in 0.5 ml of methanol).

4.3 Polystyrene

Polystyrene is an inexpensive and hard plastic vinyl polymer. As for its structure , it is a long hydrocarbon chain ,with a phenyl group attached to every other carbon atom . It is produced by free radical vinyl polymerization , from the monomer styrene.

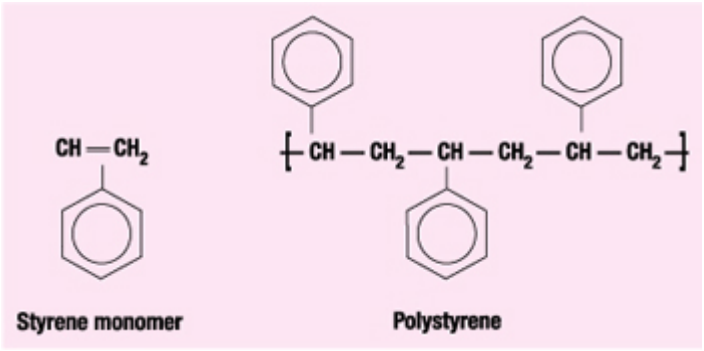

fig 9Polystyrene Structure

Polystyrene offers strength and durability without adding significant weight .Since the water absorption is so low and the compressive yield strength so high ,it provides good a protection against moisture and is able to maintain its shape for long periods of time.

Photobiotin and Avidin Chemistry

4.4.1 PhotoBiotin

It is possible to selectively attach different biological molecules in precise areas of a surface by using a combination of self-assembly and photactivation. The method is based on the interaction between streptavidin (or a deglycosylatcd form of avidin, avidin D) and of the ligand biotin, which is functionalized with a photoactive group and is thus referred to as a photobiotin.

Photobiotin is a heterobifunctional molecule which consists of three distinct regions a biotin group, a linker arm and a photoactivable aryl azide moiety.(fig 10) The biotin group is

located at the one end of the molecule and is responsible for the ability of photobiotin to interact with avidin molecules. Biotin (or vitamin H)(fig 11) is a small biologically active molecule with a molecular weight of 244,31 Da which acts as a co-enzyme in living cells. The two parts of the molecule are joined together by carbon linker.

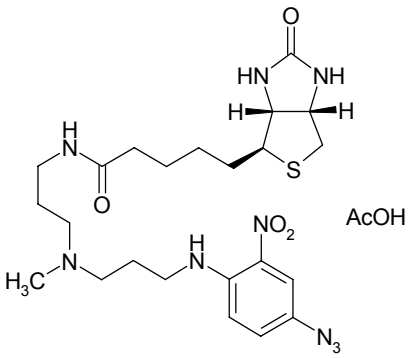

Fig 10 PhotoBiotin

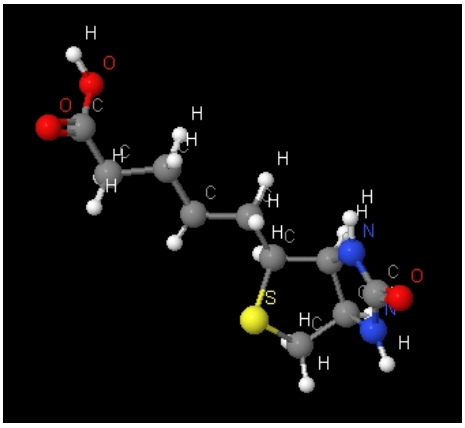

fig 11 Biotin

Upon exposure to UV light in the region 240-370nm the aryl azide converts to an aryl nitrene. This reactive species is capable of covalently attaching to C=C and C bonds. Moreover the photoactivable group undergoes photolysis to generate intermediates that can insert readily into the chemical bonds of polymer substrates.[85] (fig 12)

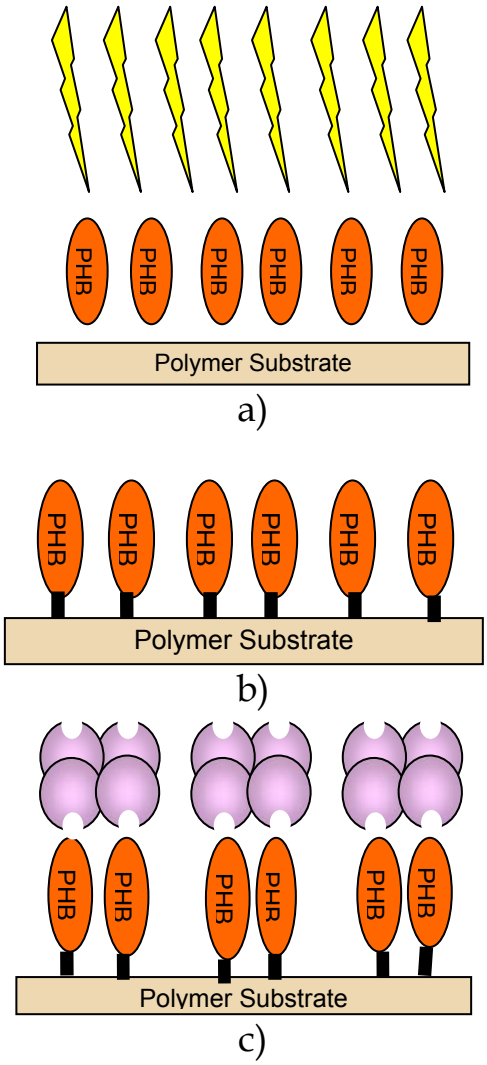

fig 12a)UV Exposion b)Binding of Photobiotin on the ORMOCER c)Binding of Photobiotin to Avidin

A wide range of macromolecules including proteins, polysaccharides and nucleic acids can be readily linked to biotin without serious effect on their biological, chemical or physical characteristics.

4.4.2 Avidin-Streptavidin

Avidin is an egg-white derived glycoprotein. Each subunit consists of 128 amino acid residues and one glycomoiety attached to Asn17. The molecular weight of avidin is about 62KDa. The tetrameric structure of avidin (has four binding sites for photobiotin) makes it possible to bind both to biotin and biotinylated molecules groups on surfaces.(fig 12 c) The avidin

molecule is like a big magnet that grabs the smaller biotin. The sandwiched structure leads to an irreversible covalent binding with a high affinity of $K_a=1x10^{-15}M^{-1}$.

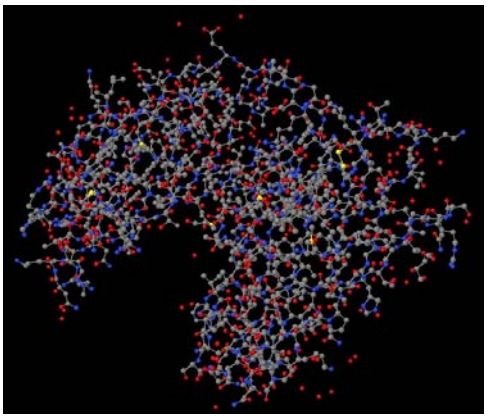

fig 13 Avidin

Streptavidin is a bacterial protein from Streptomyces avidinin. It is homologous in structure with chicken avidin . Avidin and streptavidin are both very stable proteins .Streptavidin also binds to biotin extremely tightly ,but around 100-fold less compared to avidin $K_a=1x10^{-14}M^{-1}$.[85]

Atto dyes are a comprehensive series of fluorescent dyes, which cover the entire spectrum of visible light, match the most common output wavelengths of excitation light sources but also common lasers provide brightest fluorescence with narrow fluorescence emission spectra and finally show extraordinary photostability

These properties enable the parallel imaging of different targets in cells, tissues or other biological samples. Figure 1 shows characteristic absorbance- and emission spectra of the atto dye family.

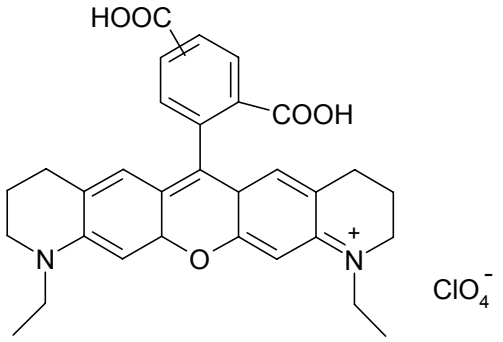

fig 14 Atto 565 Fluorescence substance

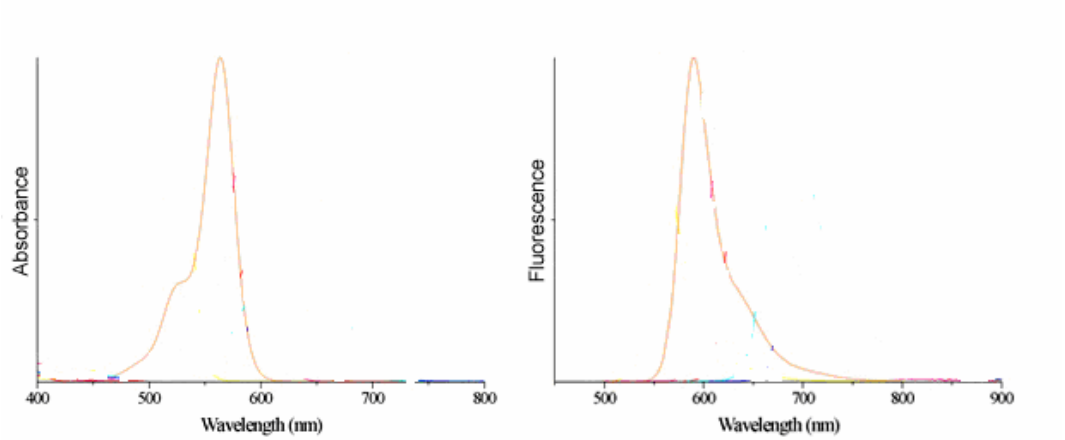

Figure 15: Absorption and emission spectra of Atto 565 Atto 565 has $\lambda_{max\ abs}$=560 nm and $\lambda_{max\ em}$=585 nm .

4.5 Protein IgG

Immunoglobulin G (IgG) is an antibody (Ab) ,which is characterized as all the antibodies do ,from its ability to recognize and bind specifically to molecules of Antigen(Ag) that offend an organism and at second to activate a line of biological molecules and cells that have aim the removal of antigen from the organism.

IgG is a protein with molecular weight ~ 150kD that is constituted from two heavy chains and two light polypeptide chains .The two heavy chains are linked with each other with disulphide bonds and each of the heavy chains are linked with the light via disulphide bond.This protein molecule presents an axis of symmetry since the two heavy, and the two light chains are identical.

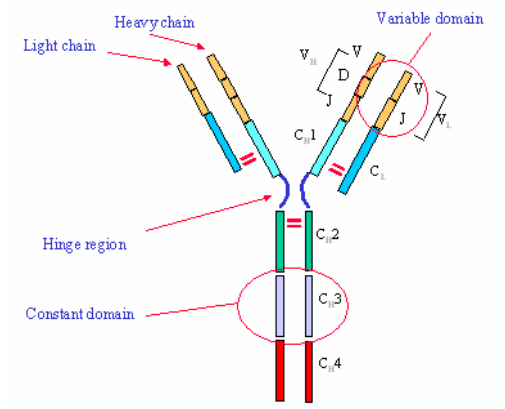

Fig 16 Structure of IgG

The importance of protein IgG is interwoven with its faculty to response immediately afterwards its excretion, in offences of organism from a line of contagious factors. This is realised via the interaction of IgG with antigens of the surface of contagious factors.

The technology of biosensors used the molecules of immunoglobulins for the creation of anoso-biosensors with various applications. One of them is the creation of amperometric anoso-sensors for the immobilisation of biotinylated immunoglobulin G from rabbit (rabbit IgG) in modified surfaces of avidin (Darain, F. et al., 2003) but also the detection rabbit IgG from anti-IgG (Gooding, J.J et al., 2004).

Chapter 5 Experimental Results

A Two Photon polymerization of an Eosin Y sensitized acrylate composite

5.1.1 Purpose

An innovative technique ,the 2PP of an acrylate composite, was developed for built 3D structures bottom up layer by layer using an infrared femtosecond laser at 1028nm . The composite consisted of an acrylate monomer, a free-radical co-initiator and a photo-sensitizer. The material was transparent to infrared laser radiation and absorbed strongly in the visible spectrum. Scanning the tightly focused laser beam, we achieved polymerization and solidification of the material. Due to their versatile optical and chemical properties and their ability of mixing with active molecules, the materials described in this work are particularly useful for a variety of applications such as photonic devices, actuators and micro-fluidic devices. In addition, as both the single photon and the two-photon wavelengths are not in the ultraviolet part of the spectrum, this technique is particularly promising for incorporation into the photo-polymer of active molecules that are sensitive to UV radiation.

5.1.2 Experimental set-up

The set-up for the fabrication of three-dimensional microstructures by two-photon micro stereolithography is shown in Fig. 1. The laser used is an Amplitude Systems t-pulse laser femtosecond oscillator operating at 1028 nm. This source is a compact diode-pumped femtosecond laser oscillator with an average lazer power of 1W delivering a series of high energy, short duration pulses of less than 200fs and a repetition rate of 50MHz.

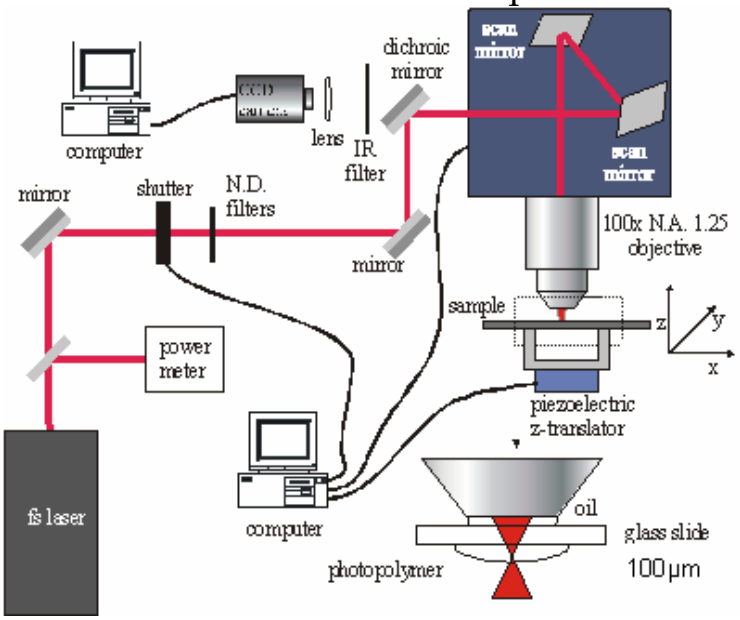

Fig. 1 Experimental set-up

By moving the laser focus in a three-dimensional manner through the liquid, three-dimensional structures can be fabricated.[87] The photopolymerized structure was generated using an x–y- galvanometric mirror digital scanner (Scanlabs Hurryscan II), controlled by SAMLight (SCAPS) software . SAMlight software allowed the drawing of varius stuctures built layer by layer .The scanner had been adapted to accommodate a high numerical aperture focusing microscope objective (Nikon 50×, N.A. = 0.8). The lateral resolution of our objective is given by :

$$r = 0.61\lambda/N.A. = 785 \text{ nm}$$

and the axial resolution by

$$r=2\lambda n/(N.A.)^2 = 3.2\mu m.$$

Movement on the z-axis was achieved by a single-axis piezoelectric stage (PI) and beam control by a mechanical shutter (Uniblitz). The piezoelectric stage and the shutter were computer controlled via a National Instruments LabVIEW program. Beam intensity was controlled using neutral density filters. A CCD camera was mounted behind a dichroic mirror for online monitoring of the two-photon polymerization process. This is made possible as the refractive index of the originally liquid photo-polymer changes during polymerization, so that the illuminated structures become visible during the building process.

5.1.3 Experimental Process-Results

The material was prepared following the reference formulation .We placed a drop in the middle of a coverslip and on the sample holder. Most important, we had to find the interface glass – substrate and this was achieved moving the laser beam at the z axis and detecting the second reflection of the focal spot .The structures were built bottom up layer by layer by repeating the same pattern over several layers depending on the desired thickness .As the material was very viscous and the build process lasted less than a minute, material drifting was not an issue.

The fabrication was controlled by three parameters ,the number of loops for each layer ,ie the number of times the scanning is repeated at a same z value ,the galvo mirror scanning speed and the power of the laser regulated by filters .Several structures were built with varying these parameters .

The first component built by two-photon polymerization consisted of 9×10 square cells array.The component was built by repeating the same pattern over 15 layers with a 1 μm separation thickness. The separation thickness was smaller than the lateral focal length of the lens therefore the adhesion between the layers was adequate.(fig 2)

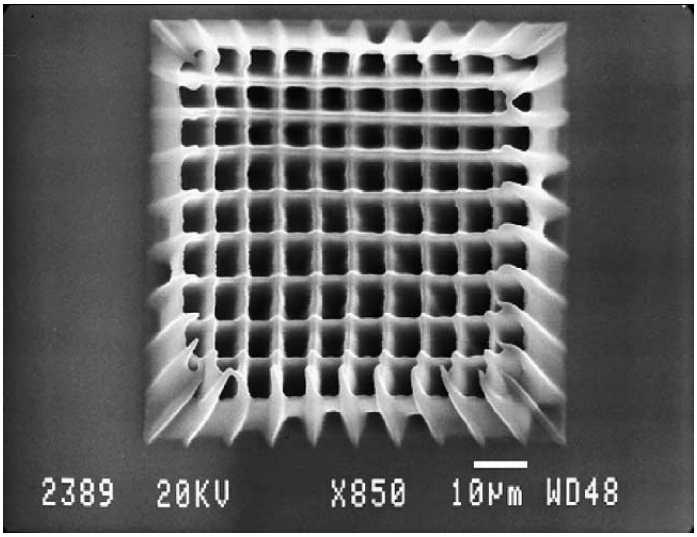

Fig. 2. SEM image of the component built by two-photon microstereolithography. 850xmagnification.

The galvo scanning speed used in all cases was 7mm/s. For the same galvo speed, several laser powers were investigated. The lowest laser energy per pulse that appeared to polymerize the material was found to be 2.5 nJ, which corresponds to a laser fluence of 0.13 J cm^{-2}. The components were made using this minimum laser pulse energy.

After the completion of the component building process, the sample was developed for approximately 20s in methanol and then it was dried. Following the washout, the samples were coated with a few nanometers thick gold-palladium layer and their structural properties were investigated in a scanning electron microscope (SEM). The gold–palladium layer is essential since the surface of the structure must be conductive for being investigated in the sem.The results are depicted in Figs 2 and 3.

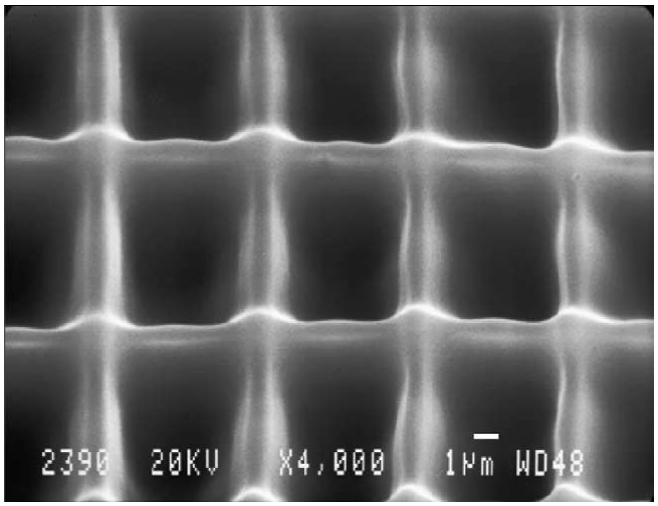

Fig. 3 A 4000xmagnification of a feature of the component of Fig. 2.

Moreover a hollow gear and a filled gear were built with the same conditions as above .

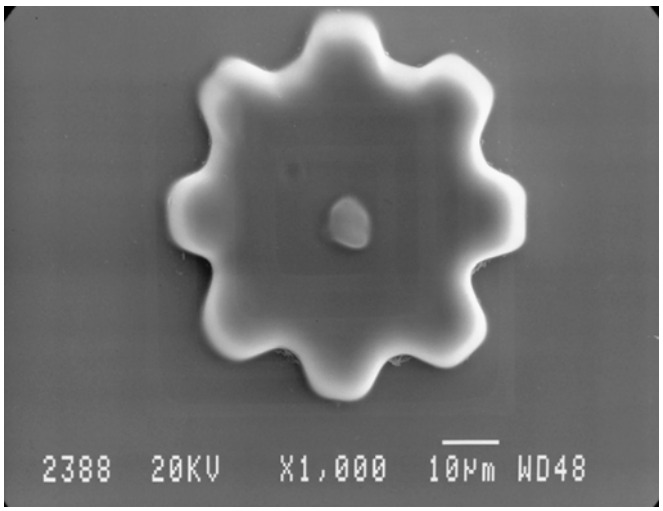

fig 4 A filled microgear

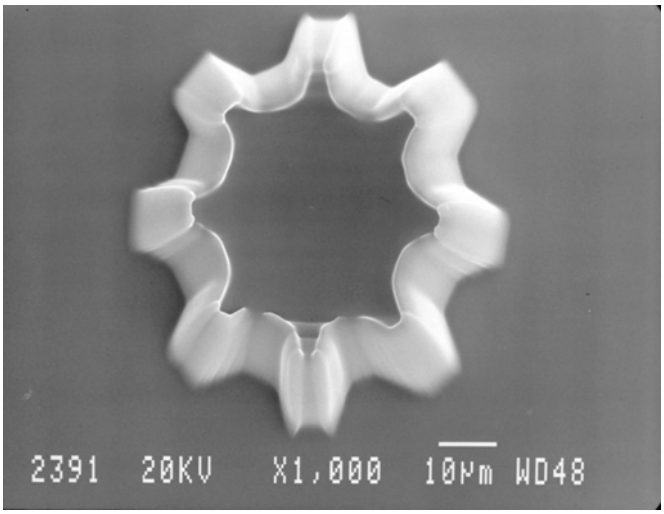

fig 5 A hollow microgear

All the components appeared to suffer from distortion due to shrinkage .This was an important problem we had to deal with during the experiments. On the materials front ,the problem is greatly reduced by using a mixture of oligomers as the polymers backbone .When oligomers are photo-polymerized the volume reduction is smaller compared to monomer polymerization .

5.1.4 Conclusions

Microstructures with dimensions of tens of microns have been built with polymer composite with a lateral resolution of 1 μm. It has been shown that the axial resolution enables the building of more complicated structures by scanning layers with different patterns. More experience on this technique and on the materials has to be acquired in order to build structures with a design giving rise to a concrete application. The material and the innovative method of two-photon polymerization are promising for the incorporation of active molecules that are sensitive to UV radiation.

B Construction of three dimensional structures by three-photon polymerization

5.2.1 Purpose

Three-photon polymerization of an organic –inorganic material known as ORMOCER was used for building 3D structures layer by layer using an infrared femptosecond laser at 1028nm. The material was transparent in the visible and near infrared ranges. By scanning the tightly focused laser beam, polymerization and solidification of material was achieved. This non linear technique of polymerization leads to the construction of photonic crystals and miniature models of very high resolution.

5.2.2 Experimental set-up

The set-up for the fabrication of three-dimensional microstructures by three photon polymerization is the same used for the 2PP .By moving the laser focus in a three-dimensional manner through the liquid, three-dimensional structures could be fabricated. The photopolymerized structure was generated using an x–y- galvanometric mirror digital scanner (Scanlabs Hurryscan II), controlled by SAMLight (SCAPS) software .SAMlight software allowed the drawing a variety of stuctures built layer by layer .The scanner had been adapted to accommodate a high numerical aperture focusing microscope objective (Edmund Scientific 100×, N.A. = 1.25). The lateral resolution of our objective is given by :

$$r = 0.61\lambda/N.A. = 501 \text{ nm}$$

and the axial resolution by

$$r=2\lambda n/(N.A.)^2 = 1.3\mu m.$$

5.2.3 Methodology- Building polymer 3D structures by three photon polymerization

a)Using objective 100X

The material was prepared following the reference formulation .A drop was placed in the middle of a coverslip and was placed on the sample holder.Moreover the most important thing was to find the interface glass – substrate which was achieved moving the laser beam at the z axis and detecting the second reflection of the focal spot . The objective of the scanner was immersed in oil for index phase matching (n_{oil}=1.515).The structures were built bottom up layer by layer by repeating the same pattern over several layers depending on the thickness desired .Fig 6[8]

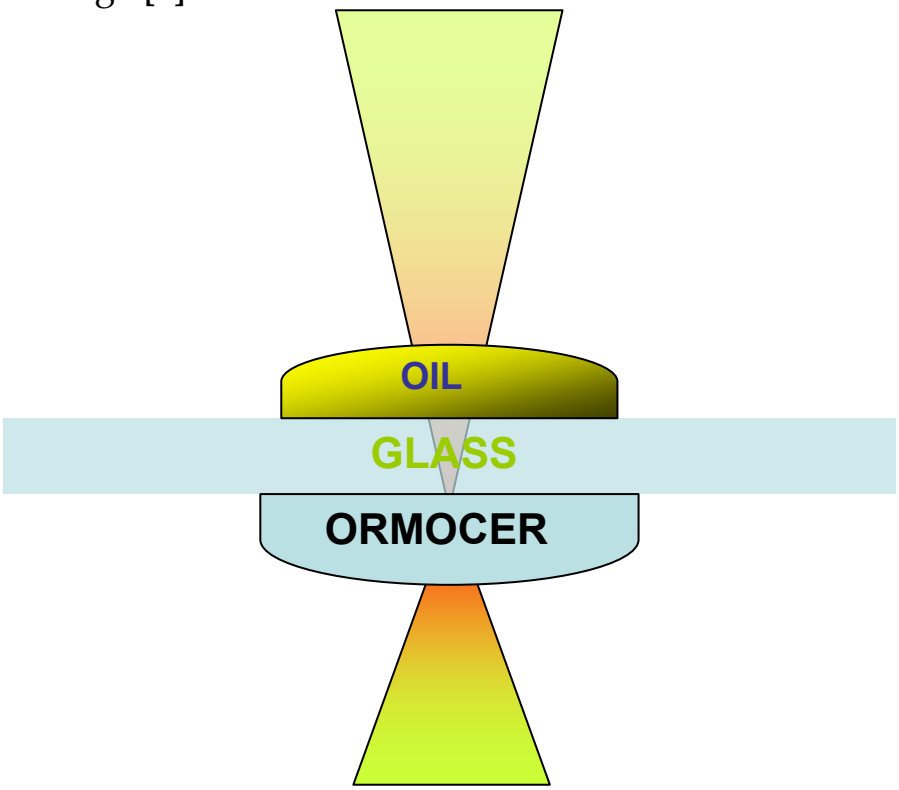

Fig 6 Laser focusing into the material

The fabrication was controlled by three parameters ,the number of loops for each layer ,ie the number of times the scanning is repeated at a same z value ,the galvo mirror scanning speed and the power of the laser regulated by filters .Several structures were built with varying these parameters .

The first component built by three -photon polymerization consisted of 5x5 square cells array (fig 7). It consisted of five step-in squares and four vertical and horizontal lines .The component was built by repeating the same pattern over 15 layers with a 1 μm separation thickness. The separation thickness was smaller than the latera focal length of the lens ,therefore there was adequate adhesion between the layers.

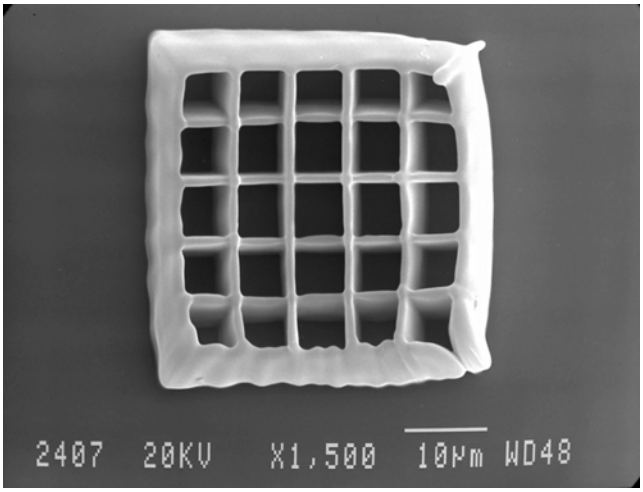

Fig 7. SEM image of the component built by three-photon microstereolithography. 1500xmagnification

The galvo scanning speed we used in all cases was 750μm/s. For the same galvo speed, several laser powers were investigated. The lowest laser energy per pulse that appeared to polymerize the material was found to be 0.8 nJ , which corresponds to a laser fluence of 0.1 J cm^{-2}. When the laser energy per pulse was increased to more than 1nJ ,the material was compromised . All the components were made using this minimum laser pulse energy.

After the completion of the component building process, the sample was developed for approximately 3 min in 50-50 solution of isopropanol ,4-methyl-2-pentanone and also rinsed in isopropanol. Following the washout the samples were coated with a few nanometers thick gold-palladium layer and their structural properties were investigated in a scanning electron microscope (SEM). The gold–palladium layer is essential since the surface of the structure must be conductive for being investigated in the sem. Figure 8 shows a 20000x magnification of the same component .It can be seen that the resolution was at least 500nm which is the

same as the focused beam waist . This clearly indicates that the effect is nonlinear and not thermal.

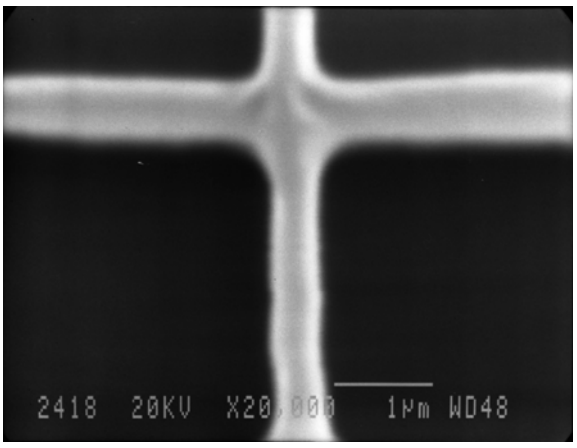

fig 8 A magnification 20000x of a feature of the component of fig 5

All the components built appeared to suffer from distortion due to shrinkage . Fig 9 shows a 1500 magnification of the component where the distortion can be clearly seen. This was an important problem we came face to face with during the experiments. On the materials front ,the problem is greatly reduced by using a mixture of oligomers as the polymers backbone .When oligomers are photo-polymerized the volume reduction is smaller compared to monomer polymerization .

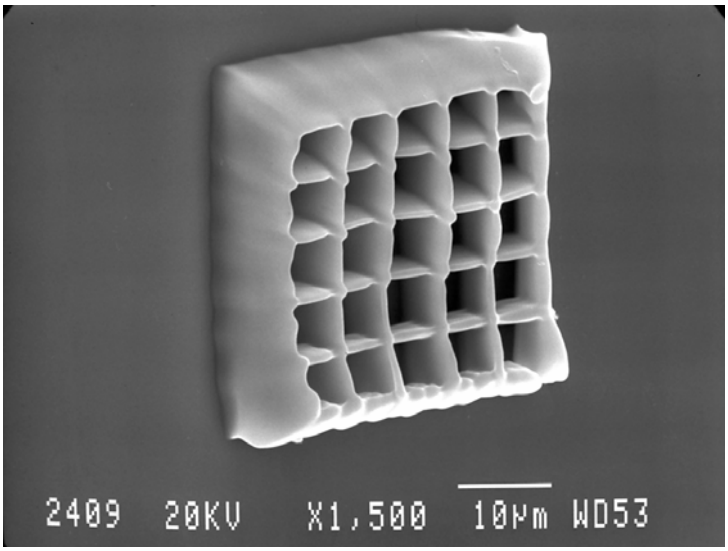

fig 9 Distortion of the component

ORMOCER containing Irgacure 369 is a material designed to be highly transparent in the visible spectrum and particularly at 514 nm ,which is the wavelength for two-photon polymerization

with our laser. In contrast, the absorption is approximately 300dB/cm at 343nm, which is the three photon polymerization wavelength for our laser.

b)Using objective 50x

ORMOCER was applied on holder following the previous process . The objective 50x was used for focusing the laser beam into the material .The galvo scanning speed was 800μm/sec,the laser energy was 0.8nJ and the laser fluence was 0.1J/cm^2 .Fig 10 shows 16 columns with 10μm thickness. The really galvo scanning was 10mm/sec for drawing a column with length 0.1mm . But the real structure had length 8μm so the galvo speed was 800μm/sec .

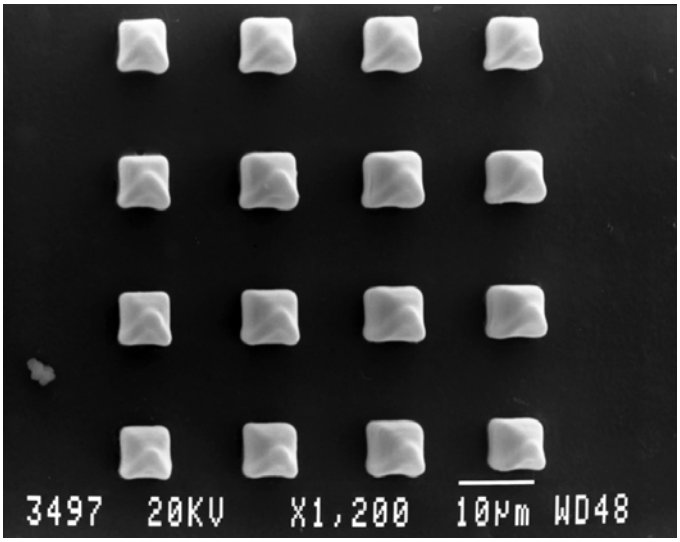

fig 10 SEM image of the columns built by three-photon stereolithography. 1200xmagnification

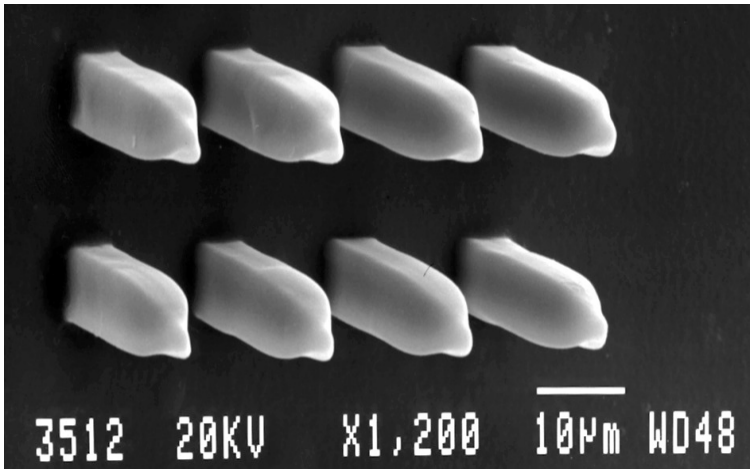

fig 11 SEM image of the columns from another view 1200xmagnification

5.2.4 Conclusions

In conclusion, we built components employing multiphoton polymerization using a compact femtosecond laser source operating at 1028 nm. This is the first time this wavelength has been employed in multi-photon polymerization (three-photon for ORMOCER®, two-photon for the acrylate-based photo-polymer). By employing multiphoton processes, we fabricated three-dimensional structures of sub-micron resolution in both materials [15].Consequently, this non-linear technique of polymerization opens the road in the construction of photonic crystals and miniature models of very high resolution.

Chapter 6 Experimental Results

A.Tracing of biomolecules interaction using an acoustic technique.

Experimental Set-up

6.1.1 SAW device

For our experiments an surface acoustic wave sensor operating at 108 MHz was used . This device was fabricated on a 0.5 mm thick piezoelectric quartz crystal, specifically a rotated Y-cut (42.5) quartz with propagation 90 deg with respect to the x-axis. The microdevice consists of a set of electrodes which are on the same surface named interdigital transducer(IDTs). The IDTs were consisted of 10/200-nm thick chromium/gold electrode and 80 pairs of split fingers with a periodicity of 45 μm.(fig1)

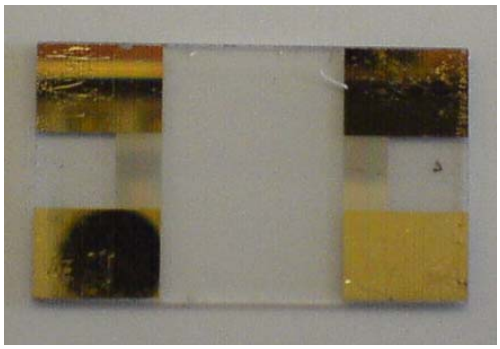

Fig 1 SAW device

On the surface of the biosensor ,where the acoustic wave is transmitted, a 1.2 μm thick waveguide layer of poly(methyl methacrylate) (PMMA) was deposited by spin coating at 4000 rpm for 40 sec with a 17% solution of medium molecular weight PMMA (Aldrich) .ThePMMA-covered devices were heated to 195 °C for 2 h to facilitate solvent evaporation. The operating frequency of the acoustic waveguide device was 105 MHz. To minimise interfering reflections during experiments the device was measured with scotch tape on the back

6.1.2 Device Holder

The biosensor was placed in a proper case (fig 2), the device holder, which consists of two golden platters and keeps it in a constant place. The flow cell is applied upon the device holder and it is placed on the free surface between the IDTs. In addition it is connected with the network analyser that measure the phase and the width of the outcoming acoustic signal .

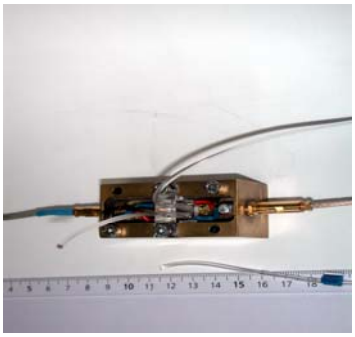

fig 2 Device holder

6.1.3 Network analyzer

In practice, the changes in the attributes at the interface are detected by measuring the amplitude and the phase of the acoustic wave. The amplitude is related to the efficiency during propagation of the acoustic wave in the surface .The amplitude is measured in dB and indicates the changes in the viscosity at the interface liquid/solid. The phase is related to the speed of the acoustic wave, substantially it is that is to say the speed with which constant point of phase of wave is transported along the propagation axes. The phase is measured in deg and the changes that are observed are related mainly to the changes of mass at the interface.

fig 3 HP 4195A Network Analyzer

A network analyzer HP 4195A (fig 3) was used for calculating the characteristics of acoustic waves over some frequencies of the applied current .Network analyser is connected with a computer in order to record the characteristics of the acoustic signal for certain frequency . During experiments a 3MHz region of the frequency spectrum near the maximum operating frequency was scanned every 43 sec to monitor the signal and collect the data.

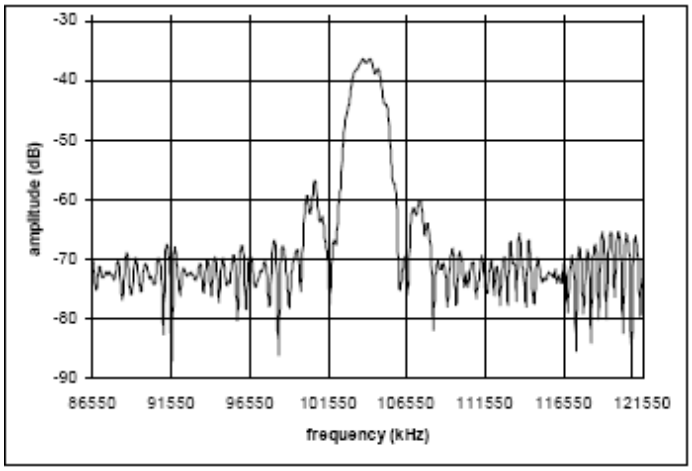

fig 4 Amplitude response of an acoustic wave for a wide range of frequencies

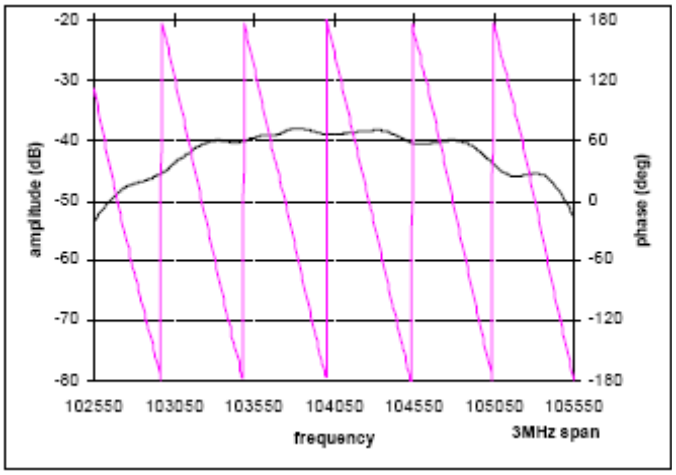

fig 5 The phase (fouxia colour) and the amplitude as they appear in network analyzer for a small spectrum of frequencies (3 MHz)

The frequency spectrum ranges from 10Hz to 500MHz with an excellent 0.001 Hz resolution for audio, baseband, HF, VHF and IF applications.

It directly measures amplitude ratio, phase, group delay and spectrum level needed for characterizing linear/non-linear analogue circuits or components used in communications, telecommunications, consumer electronics and other equipment. Furthermore, the HP 4195A has internal user functions for computing and self controlling capability.

6.1.4 Peristultic Pump-Vacuum Oven

The solutions (PBS, Avidin) that are passing from the surface of the device are transfered via a system continuous flow(flow cell)fig 6 with pipe diameter 0,25 μm. The Perspex flow cell with a silicon rubber gasket was used to hold the solution in place over the region of the device between the IDTs exposing an area of 12 mm^2. The flow cell conserves the flow of the solution at a steady rate (55μl/min). In our experiments a peristaltic pump Gilson Minipuls 3 was used.

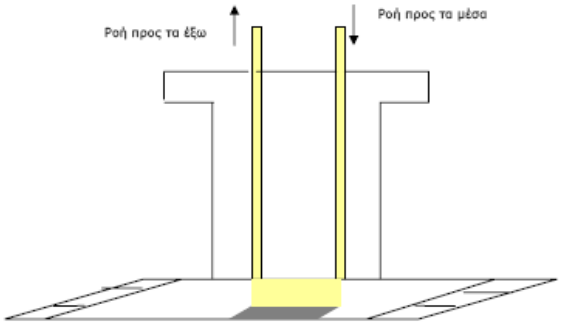

fig 6 Flow cell

In the experiments we used a vacuum oven which is ideal for drying, curing ,desiccating ,annealing and outgassing. It is configured to work with reduced pressures. For biomolecule patterning, the 3D components were covered with a photobiotin solution .The solvent was removed by drying the samples under vacuum at room temperature. Moreover after we applied photobiotin on the surface of the sensor ,it was dried under vacuum at room temperatures in the dark for approximately 1 h.

6.1.5 Preparation of PMMA waveguide

PMMA is a polymer which is the guiding layer for the acoustic waves and is used because their very low shear acoustic

velocity V_{pmma} = 1100 m s^{-1}, as compared to that of quartz V_{quartz} = 4950 m s^{-1} , (ρ=2,2 g/cm^3),results in a high energy confinement on the device surface.

In this work , PMMA 17 %(poly(methyl mathacrylate)) was applied on the acoustic device with spin coating .

For the preparation of PMMA polymer we used

- PMMA medium molecular weigth powder ,Aldrich
- 2-ethoxyethyl acetate (2-EEA) as organic solvent
- Filters with resources of diameter of 0.2 mm from PTFE membrane The polymer was mixed in a small bottle with organic solvent using a magnetic stirrer for more than two days. Then by using a glass syringe and using the above filters the solution was filtered . The PMMA solution is preserved at room temperature .

Spin coating was the preferred method for the application of thin, uniform films to flat substrates.

An excess amount of polymer solution (80 μl) is dropped with a Pasteur pipeta on the top of a substrate. The substrate is then rotated for 40 sec at high speed 4000 rpm at an angular velocity, w, in order to spread the fluid by centrifugal force, making a thin layer . The spin coater used is the Spincoater Model P6700 Series, Specialty Coating Systems Inc . The solvent was evaporated by heating the coated device in an oven at 190 ^oC for 2 h.

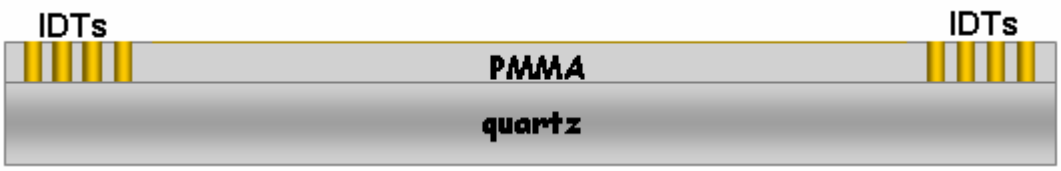

fig 7 Characteristics layers of biosensor. The PMMA layer was placed above quartz plate.

B ORMOCER Experiment

6.2.1 Purpose

The integrity of the photolytically immobilized biotin is confirmed by the detection of the binding of fluorescently labelled avidin via surface acoustic sensor technique. Biotin is subsequently immobilized on the surface of the device by excimer laser photolysis of photobiotin. The aim of this work was to find the optimum concentration of photobiotin solution which could be placed on the device, in order to fully cover the ORMOCER's surface.

6.2.2 Experimental Process

In this work , 80 µl of PMMA 17 % was applied on the acoustic device with spin coating. Then 25µl of a 1µg/ml ORMOCER solution in 4-methyl-2-pentanone solvent was applied on the device. Ormocomp USS4 (CH 23604) was purchased by Micro Resist Technology.Experimentally was proved that the forementioned ORMOCER's concentration had the greatest sensitivity for alterations that take place on the surface (mass loading) during the experiment. Then the surface was dried under a UV lamp for 30 minutes. 130 µl of Photobiotin solutions 79728 (Analysis Number 61961/1 1193) within the concentration 10-200µg/ml were applied to the device surface and were dried in a vacuum oven for one hour. Moreover the biotinylated surface of the acoustic sensor was exposed to 20 pulses of UV radiation of a KrF excimer laser (TUI Braggstar). The duration of the pulses was 7ns , the wavelength was 248nm and the energy 10-15mJ (flow rate 0.03 J/cm^2) .

The biosensor was placed in a device holder .At the beginning of each experiment PBS buffer was pumped through until a stable phase reading was obtained ,followed by injection of avidin solution and final rinse with PBS buffer .

6.2.3 Results and discuss

a) Different Solutions of ORMOCER

When a 50 μl avidin solution(1mg/ml) in 0.45ml PBS is applied on the surface of the sensor via the peristaltic pump ,the phase falls . This is illustrated in diagram 8 . It was observed that the change of phase was of the order of 1,2 deg for the 1μg/ml ORMOCER solution while this change was smaller for the other solution 10μg/ml.

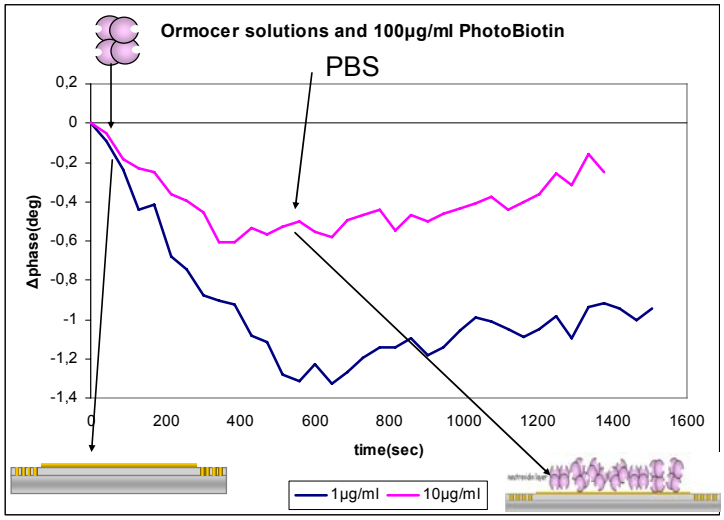

Diagram 8 Change of phase after addition of avidin solution.

b)no photobiotin

First of all, avidin was applied on the device and was found out that avidin was not fixed on the ORMOCER.(fig 9)

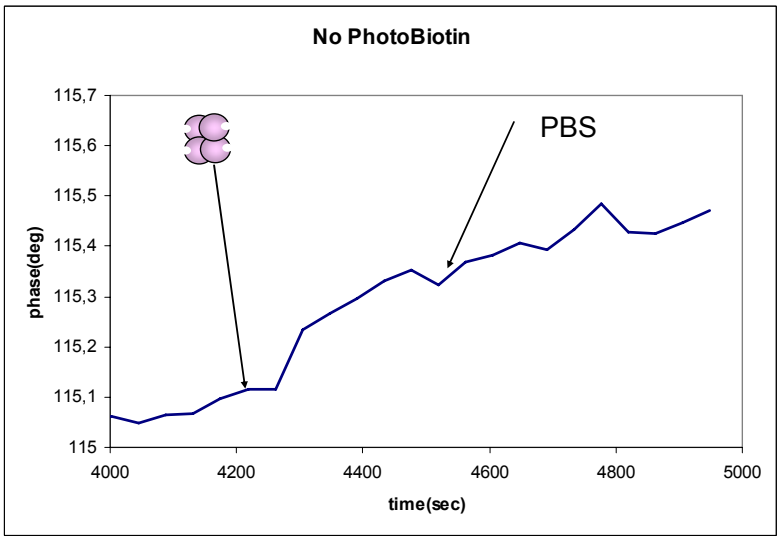

fig 9 No photobiotin

The phase of the Love wave is illustrated in fig 9 and does not change. Consequently molecules of avidin have not fixed with the molecules of ORMOCER.

c)10,50,100,200μg photobiotin/1ml

The experiment was repeated with the same conditions like before. 150μl of photobiotin with a concentration of 10μg /1ml was applied on the device. The device was immersed into the buffer solution with a flow rate of 55μl/min, and 50μl avidin 1mg/ml in 0.45ml PBS were deposited . Finally the device was immersed again into the PBS.

On the surface of ORMOCER different solutions of photobiotin were added following the above process. The phase change monitored in real time during the application of avidin on the 10 μg/ml, 50 μg/ml, 100 μg/ml and 200 μg/ml of photobiotin coated acoustic waveguide device surface is illustrated in figure 10. The special binding of streptavidin to biotinylated surface of the ORMOCER was confirmed by the phase change .

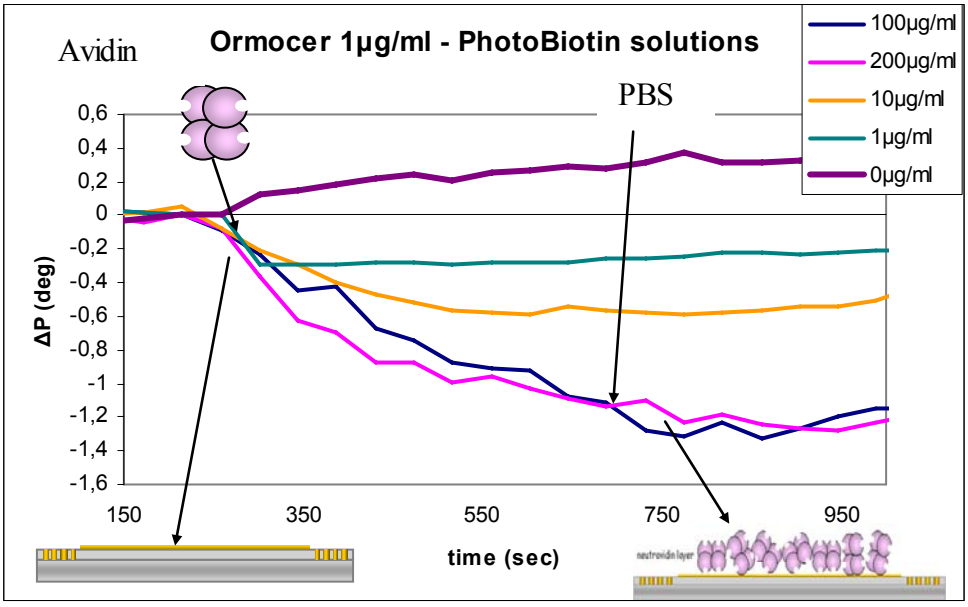

fig 10 The phase change monitored in real time during the application of avidin on the 10 μg/ml, 50 μg/ml, 100 μg/ml and 200 μg/ml of photobiotin solutions

In all the experiments that were performed under the same conditions ,it was observed a good repeatability in the phase changing when avidin solution was added, as we can see from the diagram below. (fig 11)

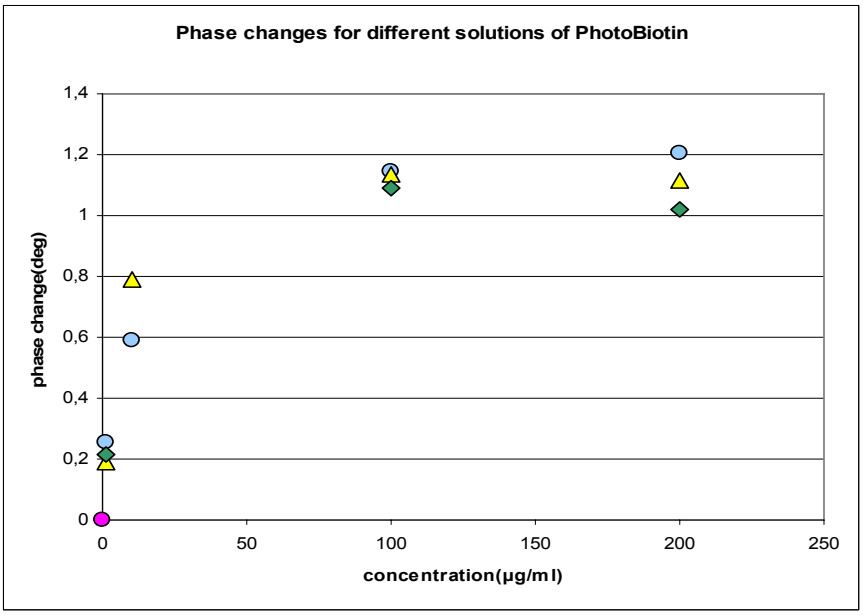

Fig 11 Phase changes for different solutions of photobiotin

It is obvious that the surface reaches saturation when a 200μg/ml solution of photobiotin is added. Moreover, the smallest detectable concentration of photobiotin's solution is 10μg/ml.

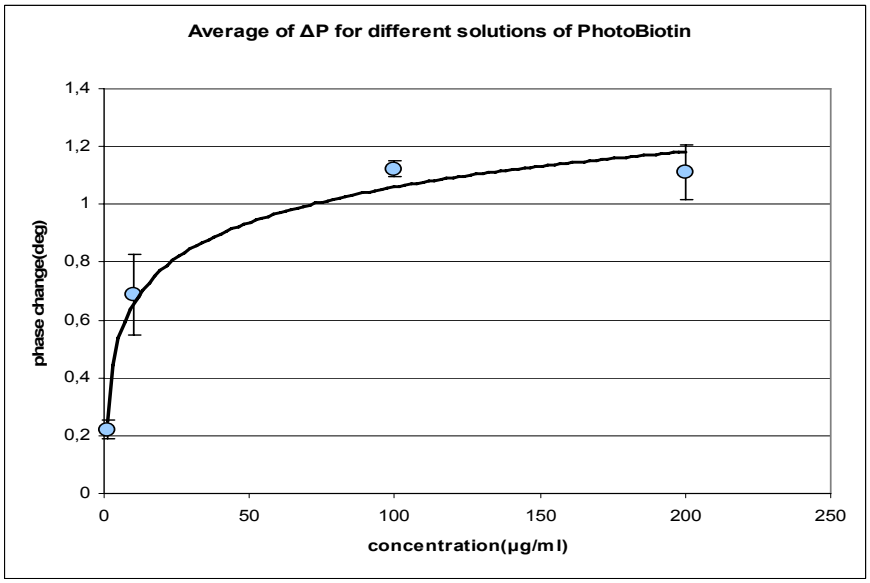

fig 12The average change of phase

6.2.4 Conclusions

In the present study, we made a first approach of the acoustic response of the biosensor at the addition increasing concentrations of photobiotin solutions that are increased. A first conclusion is that the binding of 200μg/ml photobiotin to avidin is more efficient than it is at lower concentrations.

C Polystyrene Experiment

6.3.1 Purpose

The integrity of the photolytically immobilized biotin is confirmed by the detection of the binding of the fluorescently labelled avidin via surface acoustic sensor technique. Biotin is subsequently immobilized on the surface of the device by excimer laser photolysis of photobiotin. The aim of this work was to find the optimum concentration of photobiotin solution which could be placed on the device, in order to fully cover the polystyrene surface.

6.3.2 Experimental Process

In this work , 80 µl of PMMA 17 % was applied on the acoustic device with spin coating. Then 30µl of a 0.02g/ml polystyrene solution (Catalog N. 18242-7,Cas N. 9003-53-6) in tuluol solvent was applied on the device. Then the surface was spin coated for 1 min at 4000 rpm .Thereafter the device was heated to 150 °C for 1h to facilitate solvent evaporation 130 µl of Photobiotin solutions 79728 (Analysis Number 61961/1 1193) within the concentration 10-200µg/ml were spin coated in order to create a thin layer of photobiotin.Moreover the biotinylated surface of the acoustic sensor was exposed to 20 pulses of UV radiation of a KrF excimer laser (TUI Braggstar). The duration of the pulses was 7ns , the wavelength was 248nm and the energy 10-15mJ (flow rate 0.03 J/cm^2) .

The biosensor was placed in a device holder .At the beginning of each experiment PBS buffer was pumped through until a stable phase reading was obtained ,followed by injection of avidin solution and final rinse with PBS buffer .

6.3.3 Results and discuss

a)No photobiotin

First of all, avidin was applied on the device and was found out that avidin is not fixed on the polystyrene surface.

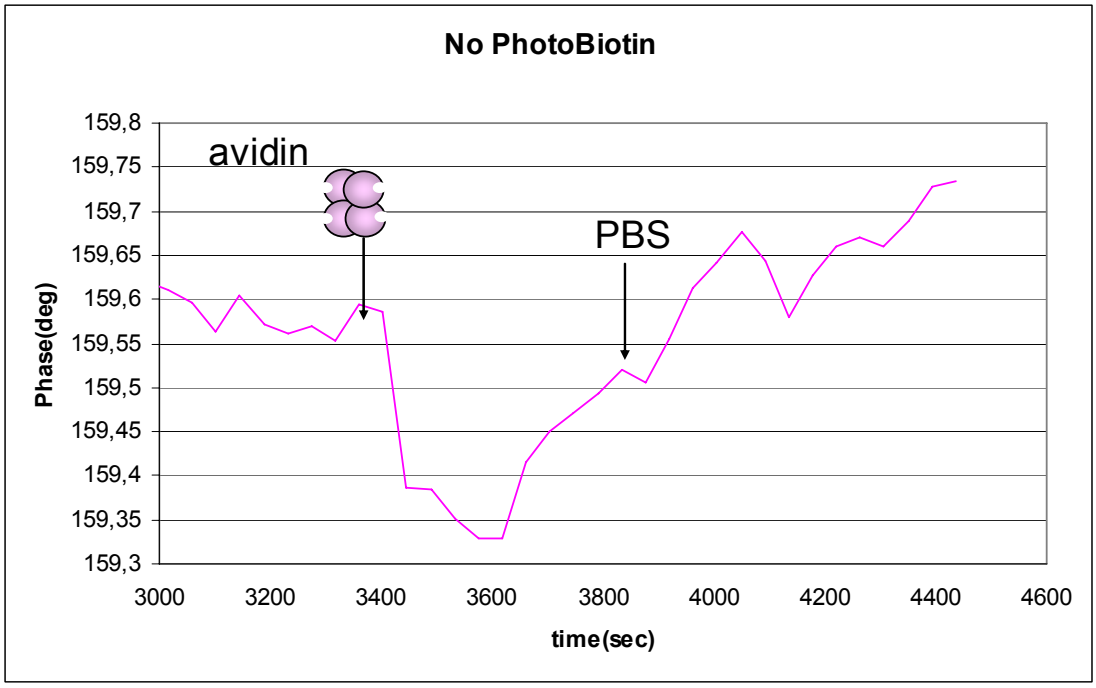

fig 13 No photobiotin on the surface of polystyrene

Figure 13 shows the phase change of the Love wave . The phase of the saw was changed but then it returned to its initial value. Consequently molecules of avidin had not fixed with the molecules of polystyrene.

b)10,20,50,75,100,200μg photobiotin/1ml

The experiment was repeated under the same conditions like before. 150μl of photobiotin with concentration of 10μg /1ml were applied on the device. The device was then immersed into the buffer solution with flow rate of 55μl/min. 50μl avidin 1mg/ml in 0.45ml PBS were then deposited. Finally the device was immersed again into the PBS.

On the surface of the polystyrene different solutions of photobiotin were added following the above process. Figure 14 shows the phase change monitored in real time during the application of avidin to the 10 μg/ml, 20 μg/ml ,50 μg/ml, 75 μg/ml ,100 μg/ml and 200 μg/ml of photobiotin coated acoustic waveguide device surface.

The special binding of streptavidin to biotinylated polystyrene's surface is confirmed by the phase change .

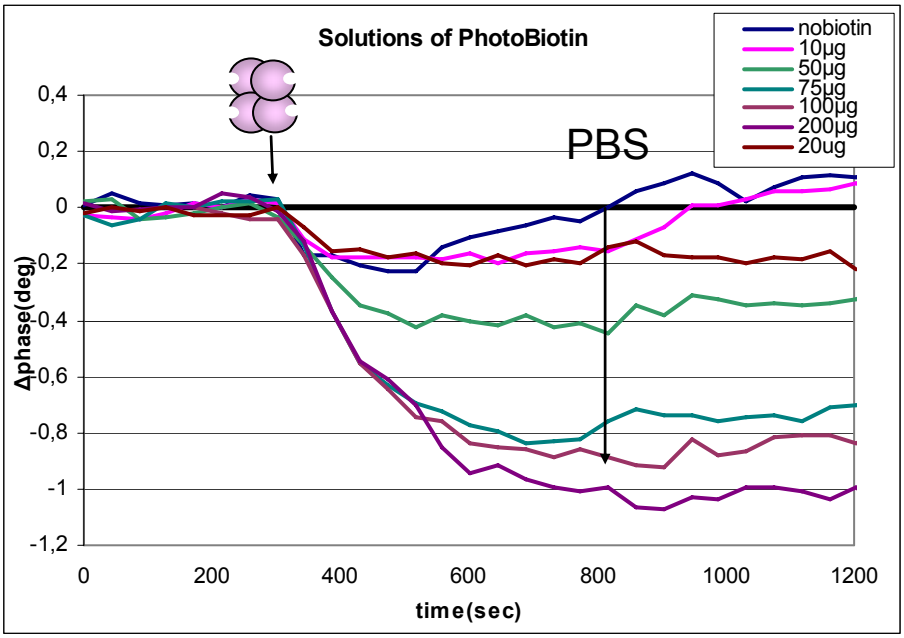

Fig 14Phase changes for different solutions of photobiotin

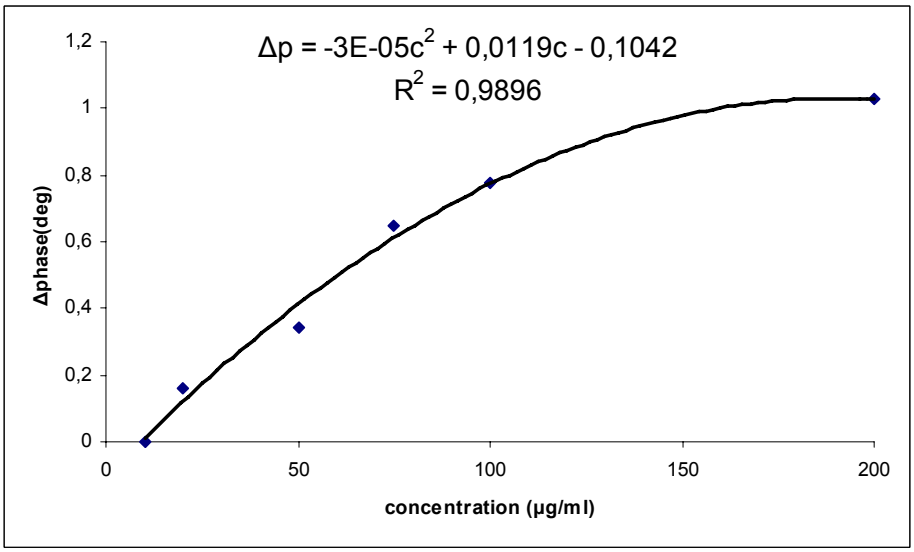

Fig 15 Change of phase as a function of concentration

It was observed that phase changing was linearly connected with concentration but only for low concentrations of

photobiotin.(fig 17). It is obvious that the surface reaches in saturation when 100 µg/ml solution of photobiotin are added .Moreover, the smallest concentration of photobiotin's solution which can be detected is 20µg/ml.

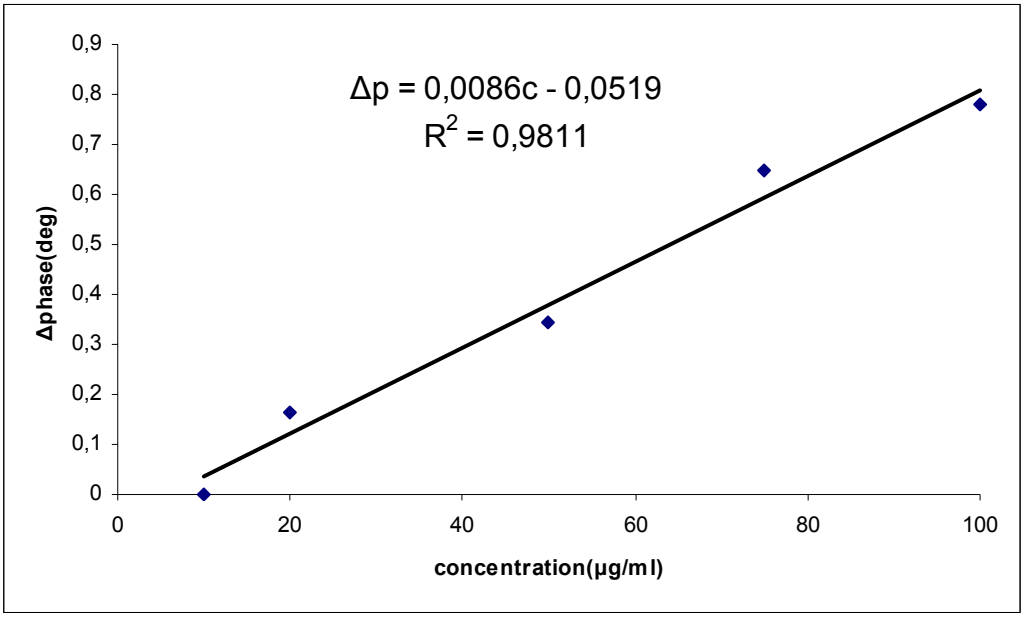

fig 16 Linear dependence Δphase with concentration of photobiotin

6.3.4 Conclusions

In the present study, we made a first approach of the acoustic response of the biosensor at the addition of photobiotin solutions with increased concentrations. A first conclusion is that the binding of 200µg/ml photobiotin to avidin is more efficient than it is at lower concentrations.

D Anti IgG Experiment

6.4.1 Purpose

The aim of this work is to enclose the biological molecules of photobiotin and avidin into 3D structures .The question is if these molecules are effective even after this polymerization techniques and the rinse of unpolymerized resin.

6.4.2 Experimental Process

In this work , 80 μl of PMMA 17 % were applied on the acoustic device with spin coating. Then 25μl of a 1μg/ml ORMOCER solution in 4-methyl-2-pentanone solvent were applied on the device. Then the surface was dried for 30 min under UV lamp.

130 μl of Photobiotin solution 79728 (Analysis Number 61961/1 1193) within the concentration 100μg/ml were applied on the surface of the device. In addition the surface was dried in a vacuum oven for one hour . Moreover ,the biotinylated surface of the acoustic sensor was exposed to 20 pulses of UV radiation of a KrF excimer laser (TUI Braggstar). The duration of the pulses was 7ns , the wavelength was 248nm and the energy 10-15mJ (flow rate 0.03 J/cm^2) . Then 100μl of avidin solution with concentration 1mg/ml were applied on the device and it was dried for one hour before it was rinsed out .

Moreover ,a drop of ORMOCER was applied on the surface of the device .By using a small glass, a stress was exerted in order to make a thin layer of ORMOCER on the surface. Finally the device was rinsed out in a 50-50 solution of 4 methyl-2 pentanone and isopropanol .

The biosensor was placed in a device holder .At the beginning of each experiment PBS buffer was pumped through until a stable phase reading was obtained ,followed by injection of anti IgG solution and final rinse with PBS buffer . 50 μl of 0,1ml/ml IgG were dissolved in 450μl phosphate buffer saline(PBS) buffer (137 mM NaCl ,2.7 mM KCl ,10mM Phosphate,pH=7.4)

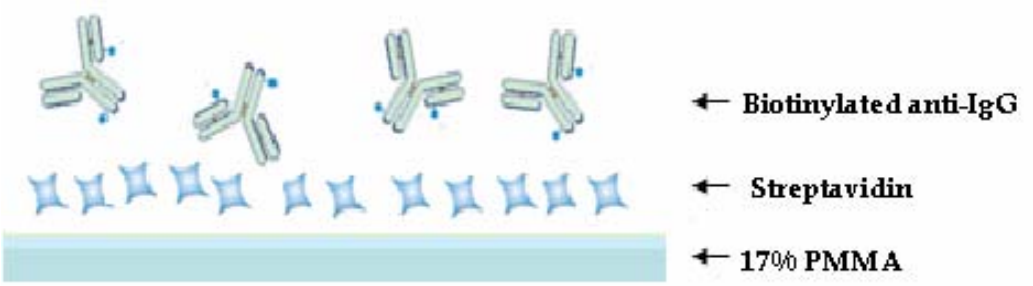

fig 17 Addition of biotinylated anti IgG

6.4.3 Results and discussion

From the experiment it was observed that avidin was not influenced by the solvents so the biotinylated anti IgG proteins were bend on the surface of the avidin .

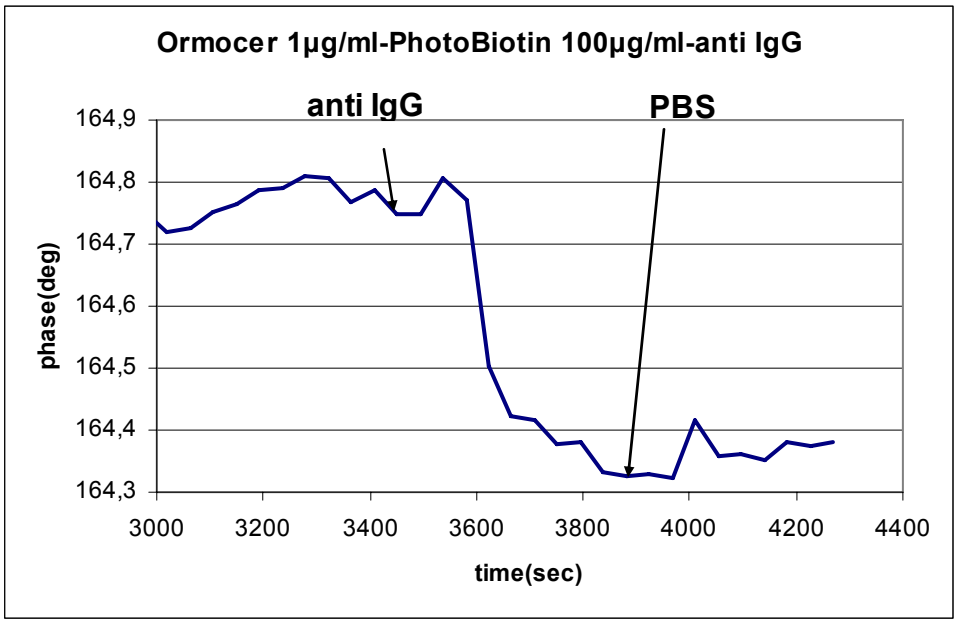

Fig 18 Anti IgG binding to avidin molecules

Tracing of biomolecules interaction using a Fluorescence Microscope

6.5 Fluorescence microscope

After building, the samples were inspected in a fluorescence microscope and some of them were found to fluorescence in green.

Further investigations showed that this fluorescence is only observed from the samples made with ORMOCER that is more that six months old. This fluorescence is most likely due to degradation products of the photoinitiator. For all the structures fabricated in study, only fresh ORMOCER has been used and control samples made to confirm that there is no fluorescence from the base material.

For biomolecule patterning, the 3D components were covered with a photobiotin solution consisting of 1mg of photobiotin in 1 ml distilled water and 1 ml ethanol .The solvent was removed by drying the samples under vacuum at room temperature in the dark for 1 h . Subsequently, the samples were exposed to 20 pulses ,1 Hz repetition rate UV radiation from an excimer KrF laser, 248 nm wavelength (TUI Braggstar,7ns pulse duration) . After the samples were rinsed with de-ionized water, they were covered in an Atto 565-Streptavidin solution (0,1 mg/ml) and was left to incubate for at least one hour. Finally they were washed in DI water in an ultrasonic bath for 10 min .

The 3D structures were imaged using a fluorescence microscope Nikon Eclipse E800 equipped with a camera and a green filter G-2A (510-560)nm. We found, that they fluoresce very strongly, when was excited with green light. This fluorescence originates from the 3D component (and not from the glass substrate)(fig 19) .Since ORMOCER and photobiotin do not fluoresce in the green, fluorescence can be safely ascribed to the Atto 565-streptavidin .

For the samples which are not pre-treated with photobiotin and only treated with avidin there was no fluorescence (Figure 20). Therefore, the incorporation of avidin is due to the biotin bound to the structure. Similarly, no fluorescence is detected if in the procedure biotin instead of photobiotin is employed. This result demonstrates that the biotin and avidin are not simply

incorporated within a porous structure; instead, chemical bonding is involved. Upon UV irradiation, photobiotin is known to generate a reactive biotin. It is likely that this intermediate reacts with dangling Si-O bonds at the surface of the polymerized structure.

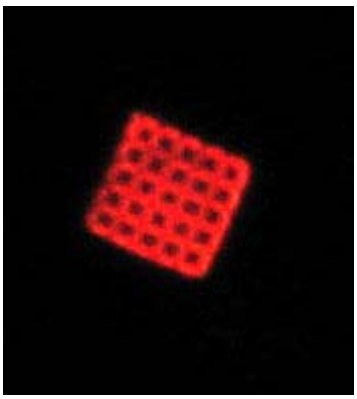

fig 19

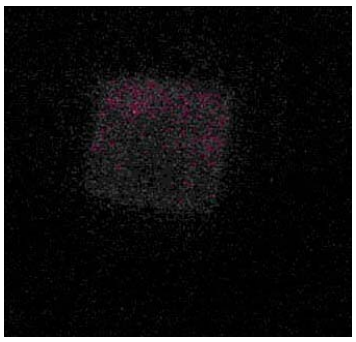

fig 20

The molecules of avidin are deposited not only on the top of the structure but at the lateral walls also ,as we can see in fig 21.

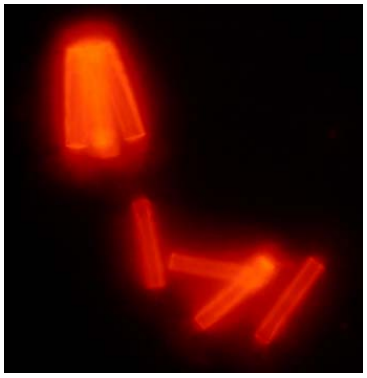

fig 21

Chapter 7 Conclusions - Future plans

7.1 Conclusions

A new technique has been presented for three dimensional biomolecule patterning, based on multi-photon polymerization and biotin-avidin chemistry. Three-dimensional structures have been built employing multi-photon polymerization and photolytic attachment of biotin active molecules on them. Microstructures with dimensions of tens of microns have been built with different materials with a lateral resolution of 1 μm. It has been shown that the axial resolution enables building more complicated structures by scanning layers with different patterns. More experience on this technique and on the materials has to be acquired in order to build structures with a design giving rise to a concrete application.

The results have been confirmed using fluorescence microscopy and acoustic sensor techniques.A good understanding of the possibilities of acoustic wave sensing was acquired in order to understand and analyse the interactions with polymer films. Several experiments were performed with encouraging results for using this technique to sense phase change of acoustic waves induced by biomolecular interactions. An interesting result that was obtained is the observation that the photobiotin and avidin molecules are effective even after polymerization techniques and the rinse of unpolymerized resin.

7.2 Future work

The long-term goals of the project include the calibration of the technique, using fluorescence microscopy and acoustic sensor techniques.The problem that we have to overcome is the sensitivity of the acoustic sensors on the changes of the temperatrure. Investigation of selective attachment of other biotinylated molecules on the 3D structures is of great interest .

The ultimate purpose of this project is to build fully-functional 3D biosensors based on microcantilivers. They have recently become a promising tool for directly detecting biomolecular interactions with great accuracy. Microcantilevers

translate molecular recognition of biomolecules into nanomechanical motion that is commonly coupled to an optical or piezoresistive read-out detector system. Biosensors based on cantilevers are a good example of how nanotechnology and biotechnology can go together. High-throughput platforms using arrays of cantilevers have been developed for simultaneous measurement and read-out of hundreds of samples. However, besides the excellent results obtained with existing sensor technologies, we still need biosensors able to detect, in a direct way, very low (picomolar to femtomolar) levels of a great number of chemical and biochemical substances in areas such as environmental monitoring, industrial and food processing, healthcare, biomedical technology, and clinical analysis.

Microcantilevers can transduce a number of different phenomena, such as changes of mass, temperature, heat, or stress, into bending (static mode) or a change in resonant frequency (dynamic mode) , which can be monitored. Adsorption of molecules, when they are restricted to one of the cantilever surfaces, produces differential surface stress that bends the cantilever. At the same time, the resonant frequency of the cantilever also varies due to mass loading. Changes in resonant frequency can be detected by measuring the thermal noise of the cantilever.

REFERENCES

[1] S. Fodor, J. Read, M. Pirrung, L. Stryer, A. Lu, and D. Solas, Science 251, 767, (1991).
[2] S. W. P. Turner, M. Cabodi, and H. G. Craighead, Phys. Rev. Lett. 88, 28103 (2002).
[3] B. R. Ringeisen, J. Callahan, P. K. Wu, A. Pique, B. Spargo, R. A. McGill, M. Bucaro, H. Kim, D. M. Bubb, and D. B. Chrisey, Langmuir 17, 3472 (2001).
[4] L. F. Rozsnyai, D. R. Benson, S. P. A. Fodor, and P. G. Schultz, Ang. Chem. Int. Ed., 759 (1992).
[5] H. J. Choi, N. H. Kim, B. H. Chung, and G. H. Seong, Anal. Biochem. 347, 60 (2005).
[6] N. C. Seeman, Nature 421, 427, (2003).
[7] J. Serbin, A. Ovsianikov, and B. Chichkov, Opt. Express 12, 5221 (2004).
[8] M. Farsari, G. Filippidis, and C. Fotakis, Opt. Lett. 30 3180 (2005).
[9] A. C. Forster, J. L. McInnes, D. C. Skingle, and R. H. Symons, Nucleic Acids Res., 3, 745, (1985).
[10] E. Gizeli, Smart Mater. Struct., 6, 700 (1997)
[11]. Maruo S, Nakamura O, Kawata S (1997) Opt Lett 22:132
[12] Parthenopoulos DA, Rentzepis PM (1989) Science 245:843
[13] Kawata S, Sun HB, Tanaka T, Takada K (2001) Nature 412:697
[14]Pao YH and Rentzepis PM (1965) Appl Phys Lett 6:93
[15] Boyd RW (1992) Nonlinear optics. Academic, San Diego
[16]Denk W, Strickler JH, Webb WW (1990) Science 248:73
[17] Bhawalkar JD, He GS, Prasad PN (1996) Rep Prog Phys 59:1041
[18] Saeta P, Wang JK, Siegal Y, Bloembergen N, Mazur E (1991) Phys Rev Lett 67:1023
[19] Glezer EN, Milosavljevic M, Huang L, Finlay RJ, Her TH, Callan JP, Mazur E (1996) Opt Lett 21:2023
[20] Odian G (1991) Principles of polymerization, 3rd edn. Wiley, New York
[21]Glezer EN, Mazur E (1997) Appl Phys Lett 71:882
[22] Maruo S, Ikuta K (2002) Sensor Actuat A-Phys 100:70
[23] Hopfield JJ, Worlock JM, Park KJ (1963) Phys Rev Lett 11:414
[24] Kaiser W, Garrett CGB (1961) Phys Rev Lett 7:229
[25] Maruo S, Ikuta K (2000) Appl Phys Lett 76:2656

[26]. Pao YH and Rentzepis PM (1965) Appl Phys Lett 6:93
[27] Li CD, Luo L, Wang SF, Huang WT, Gong QH, Yang YY, Feng SJ (2001) Chem PhysLett 340:444
[28] Belfield KD, Schafer KJ, Mourad WJ (2000) J Org Chem 65:4475
[29] Brodeur A, Chin SL (1999) J Opt Soc Am B 16:637
[30] Stuart BC, Feit MD, Herman S, Rubenchik AM, Shore BW, Perry MD (1996) Phys Rev B 53:1749
[31] vonderLinde D, Schuler H (1996) J Opt Soc Am B 13:216
[32] Witzgall G, Vrijen R, Yablonovitch E, Doan V, Schwartz BJ (1998) Opt Lett 23:1745
[33] Flory PJ (1952) Principles of polymer chemistry. Cornell University Press, New York
[34] Higurashi E, Sawada R, Ito T (1998) Appl Phys Lett 72:2951
[35] Gauthier RC (1995) Appl Phys Lett 67:2269
[36] Galajda P, Ormos P (2001) Appl Phys Lett 78:249
[37] Sun HB, Takada K, Kawata S (2001) Appl Phys Lett 79:3173
[38] J. D. Pitts, P. J. Campagnola, G. A. Epling, S. L. Goodman, Macromolecules 2000, 33, 1514.
[39] B. H. Cumpston, S. P. Ananthavel, S. Barlow, D. L. Dyer, J. E. Ehrlich, L. L. Erskine, A. A. Heikal, S. M. Kuebler, I. Y. S. Lee, D. McCord- Maughont, J. Qin, H. Rockel, M. Rumi, X.-L.Wu, S. R. Marder, J. W. Perry, Nature 1999, 398, 51
[40] H. B. Sun, S. Matsuo, H. Misawa, Appl. Phys. Lett. 1999, 74, 786.
[41] H. B. Sun, V. Mizeikis, Y. Xu, S. Juodkazis, J. Y. Ye, S. Matsuo, H. Misawa,Appl. Phys. Lett. 2001, 79, 1.
[42]. M. Straub, L. H. Nguyen, A. Fazlic, and M. Gu, Opt.
Mater. 27, 359 (2004).
[43]. J. Serbin, A. Ovsianikov, and B. Chichkov, Opt.
Express 12, 5221 (2004).
[44] S. Kawata, H. B. Sun, K. Tanaka, K. Takada, Nature 2001, 412, 697.
[45]. M. Deubel, G. v. Freymann, M. Wegener, S. Pereira, K.Busch, and C. M. Soukoulis, Nat. Mater. 3, 444 (2004).
[46] H.-B. Sun, S. Matsuo, and H. Misawaa, Appl. Phys.
Lett. 74, 786 (1999).
[47]. P. Galajda and P. Ormosa, Appl. Phys. Lett. 78, 249
(2001).

[48]. H.-B. Sun, K. Takada, and S. Kawata, Appl. Phys. Lett.79, 3173 (2001).
[49]. T. Tanaka, H.-B. Sun, and S. Kawata, Appl. Phys. Lett. 80, 312 (2002).
[50] Advanced Materials 14 271
[51] W. G. Cady, Phys. Rev., 17, pp.531, 1921
[52] R. M. White and F. W. Voltmer, "Direct Coupling to Surface Acoustic Wave", Appl. Pys.Lett. 7, pp.314, 1965
[53] W. H. King, "Piezoelectric sorption detector", Anal. Chem. 36, pp.1735, 1964
[54] H. Wohltjen and R. Dessy, Anal. Chem., 51, pp.1458, 1979
[55] H. Wohltjen and R. Dessy, Anal. Chem., 51, pp.1470, 1979
[56] Q. Jiang, X. M. Yang, H. G. Zhou and J. S. Yang, "Analysis of Surface Acoustic Wave Pressure Sensors", Sensor & Actuators A 118, pp.1, 2005
[57] C. Y. Shen, C. P. Huang and H. C. Chuo, "The Improved Ammonia Gas Sensors Constructed by L-glutamic Acid Hydrochloride on Surface Acoustic Wave Devices",Sensor & Actuators B 84, pp. 231, 2002
[58] N. D. Dominique and P. E. Fabienne, "Polyaniline as a New Sensitive Layer for GasSensors", Analytica Chimica Acta 475, pp.1, 2003
[59] T. Wessa, M. Rapp and H. Sigrist, "Immunisensing of Photoimmobilized Proteins on Surface Acoustic Wave Sensors", Colloids and Surfaces B: Biointerfaces 15, pp.139, 1999
[60] "Acoustic Wave Sensors Theory ,Design and Physico-Chemical Applications " D.S.Ballantine ,R.M.White ,S.J.Martin , E.T.Zellers
[61] "Elastic waves in solids" A.H.Harker, British Gas
[62] Ballantine, D. S.; White, R. M.; Martin, S. J.; Ricco, A. J.; Zellers, E. T.; Frye,G. C.; Wohltjen, H. *Acoustic Wave Sensors*; Academic Press: New York, 1997.
[63] Analytical chemistry 2000 71 5967
[64] J.Phys.D.Apply.phys 33 3053
[65] Sensors and Actuators B,6 p131
[66] S.3. Martin, A.J. Ricco, T.M. Niemczyk, G.C. Frye, Characterization of { SH} acoustic plate mode liquid sensors, Sensors and Actuators 20 (1989) 253-268
[67] Sensors and Actuators A 68 (1998) 275-281

[68] Kovacs, G., Vellekoop, M.J., Haueis, R., Lubking, G.W., Venema, A., *Sens. Actuators A* 43 (1994) 38–43.
[69]. Anal. Chem. 2003, 75, 835-842
[70] R.J.Narayan,C.M.Jin,T.Partz,A.Doraiswamy Modi , D.B.Chrisey ,Y.Y.Su,S.J.Lin, A. Ovsianikov , B .Chichkov,Adv.Mater.Processes 2005,163,39
[71]. Popall, M.; Dabek, A.; Robertsson, M. E.; Valizadeh,S.; Hagel, O. J.; Buestrich, R.; Nagel, R.; Cergel, .; Lambert, D.; Schaub, M. Mol Cryst LiqCryst 2000, 354, 123–142.
[72] Inorganic–organic hybrid materials for application in optical devices R.Houbertz *, a, G.Domanna, C.Cr onauera, A.Schmitt a, H.Martin a, J.-U. Parkb Thin Solid Films 442 (2003) 194–200
[73] Current Opinion in Solid State and Materials Science 4 (1999) 571–580
[74] J. Serbin, A. Ovsianikov, and B. Chichkov, "Fabrication of woodpile structures by two-photon polymerization and investigation of their optical properties," Optics Express 12, 5221-5228 (2004)
[75] Serbin, A. Egbert, A. Ostendorf, B. N. Chichkov, R. Houbertz, G. Domann, J. Schulz, C. Cronauer, L. Fröhlich, and M. Popall, "Femtosecond laser-induced two-photon polymerization of inorganic–organic hybrid materials for applications in photonics," Optics Letters 28, 301-303 (2003
[76]Laser processing of advanced biomaterials" Adva.Mat.Proc 2005 39
[77]S. Kawata, H.-B. Sun, T. Tanaka, and K. Takada, Nature 412, 697 (2001).
[78] S. Maruo and S. Kawata, IEEE J. Microelectromech. Syst. 7, 411 (1998).
[79]. H.-B. Sun, K. Takada, and S. Kawata, Appl. Phys. Lett. 79, 3173 (2001).
[80]. H.-B. Sun, T. Kawakami, Y. Xu, J.-Y. Ye, S. Matuso,H. Misawa, M. Miwa, and R. Kaneko, Opt. Lett. 25,1110 (2000).
[81]. H.-B. Sun, T. Tanaka, K. Takada, and S. Kawata, Appl.Phys. Lett. 79, 1411 (2001).
[82] Two-photon polymerization of an Eosin Y-sensitized acrylate composite Journal of Photochemistry and Photobiology A: Chemistry xxx (2005)
[83] A. Espanet, C. Ecoffet, D.J. Lougnot, PEW: photopolymerization by 228 evanescent waves. II. Revealing

dramatic inhibiting effects of oxygen at 229 submicrometer scale, J. Polym. Sci.: Part A: Polym. Chem. 37 (1999) 230 2075–2085.
[84]http://www.ce-mag.com/archive/01/Spring/Rosner.html
[85]Covalent DNA immobilization on polymer-shielded silver-coated quartz crystal microbalance using photobiotin-based UV irradiation BIOCHEM BIOPH RES CO 290 (3): 962-966 JAN 25 2002
[86] Molecular patterning on carbon based surfaces through photobiotin activation† Analyst 126 ,195
[87]Two-photon polymerization of an Eosin Y-sensitized acrylate compositeJournal of Photochemistry and Photobiology A: Chemistry xxx (2005) xxx–xxx